Materials Chemistry and Physics 343 (2025) 131035

Contents lists available at ScienceDirect

Materials Chemistry and Physics

journal homepage: www.elsevier.com/locate/matchemphys

Polymeric and mixed-matrix membrane flat sheets in O_2/N_2 gas separation: Recent advances, magnetism concepts, and future perspectives

Nahid Nikpour [a,*], Amir H. Montazer [b]

[a] Department of Physics, University of Kashan, Kashan, Iran
[b] Department of Medical Equipment Technology Engineering, Al-Hadba University, Mosul, Iraq

HIGHLIGHTS

- Formation, structure, and O_2/N_2 separation properties of a wide variety of polymeric flat sheet membranes are reviewed.
- Roles of various additives, fillers and treatments in permeability and selectivity of the membranes are discussed.
- Basic concepts of magnetism are discussed for O_2/N_2 separation properties.
- Effect of external magnetic fields during fabrication and separation on O_2/N_2 permeability and selectivity is highlighted.

GRAPHICAL ABSTRACT

ARTICLE INFO

Keywords:
Oxygen enrichment
Polymeric membranes
Magnetic nanoparticles
Mixed-matrix membranes
O_2/N_2 gas separation

ABSTRACT

Membrane technology has opened a new horizon to oxygen enrichment research studies in order to separate this gas from other gases in the air such as nitrogen. This technology has become popular due to its low cost, low energy consumption, and easy access. Recent events in the world and bitter experience of Covid-19 and SARS epidemics have made human society face the challenge of finding a way to fabricate simple and cost-effective oxygen devices and ventilators. From a medical perspective, oxygen separation can be useful for treating aspiration and breathing difficulties. Also, nitrogen gas is required in the food industry and pharmaceutical chemicals. In this review, we provide an overview of polymeric membrane structures, and focus on organic and inorganic compound fillers in membranes. Particular attention is paid to the role of magnetic nanoparticle fillers with different concentrations, sizes, coercivity, and accumulation in mixed-matrix membranes (MMMs), while also investigating synergistic effects of magnetic modules. The roles of external magnetic field and magnetic module are also highlighted in the fabrication and testing processes. Finally, the results of O_2/N_2 gas separation using polymeric and MMM flat sheets are presented and compared, thereby determining future perspectives.

* Corresponding author.
E-mail address: nikpor.physic.solid93@gmail.com (N. Nikpour).

https://doi.org/10.1016/j.matchemphys.2025.131035
Received 20 October 2024; Received in revised form 24 April 2025; Accepted 17 May 2025
Available online 19 May 2025

1. Introduction

Membrane technology has provided a cost-effective and efficient way to separate oxygen (O_2) and nitrogen (N_2) gases from each other, according to medical and chemical industries' needs [1]. These involve the use of O_2 in gasification, oxy-combustion, desulfurization production, production of glass, welding process, sewage treatment [1] gas sensors [2,3], and nanocomposites [4,5]. O_2 gas can also be employed in medicine for oxygen therapy and help cure the breathing problems in lung infection diseases [6], while also reducing the wound area of venous leg ulcer [7], improving pulmonary hypertension [8], and treating Alzheimer's disease [9]. The N_2 gas is used in food industry, coolants, and pharmaceutical chemicals.

Despite the success of pressure swing adsorption (PSA) and cryogenic distillation methods to separate O_2 and N_2 gases, they require costly compression and cooling systems [10]. In cryogenic distillation, some of the components such as water, carbon dioxide, and hydrocarbons vanish when compressed air is passed through an absorbent. In fact, air is cooled to about 100 K in the cryogenic chamber, and enters the distillation system. Due to the difference in boiling points of oxygen and nitrogen, these two gases are separated from each other [10]. On the other hand, the PSA method is based on high pressure absorption at low pressure release [10].

In recent decades, polymeric membranes have become popular because of their flexible molding and casting. Moreover, the membrane technology can reduce the overall energy consumption of the fabrication process by 50 % [11]. The membranes are fabricated in two main geometries: flat sheet and cylinder (hollow fiber form) [12]. Polymeric membrane fabrication methods have been performed by the phase inversion process, precipitation by solvent evaporation, coating, interfacial polymerization, plasma polymerization, graft polymerization, particle leaching, track etching, etc. [12]. On the other hand, a variety of methods has been used to fabricate mixed-matrix membranes (MMMs), including the physical blending, sol–gel, infilltration, in situ polymerization, chemical atomic layer deposition, layer-by-layer assembly, etc. [12].

The commonly used method for the synthesis of magnetic membranes is the physical blending. In this method, the fillers are prepared in advance, dispersed into the polymer matrix by solution blending or melt blending, followed by polymer solidification. The filler size, polymer–filler interfacial morphology, and filler agglomeration are important factors in membrane fabrication, affecting the gas separation properties [13].

The polymeric membranes are affected by several properties of polymers in gas transportation, including morphology (hyperbranched, amorphous, dense, and porous structures) [14], unoccupied space in the atomic network structure [15], polymer polarity, d-spacing (i.e., the intersegment space in polymer chains), free volume (FV), crosslinking (degree of crystallization), molecular weight distribution, fabrication process (temperature, humidity, dried time, and removal of solvent), transition temperature, external field (magnetic and electric fields), interface defects, solubility (involving interactions between gas and polymer), local polymer dynamics, etc. [16].

Most of the membranes employed in gas separation utilize glassy polymers due to their high selectivity and mechanical resistance [17]. Some results have indicated that gas separation factors such as permeability and selectivity are sensitive to the presence of low molecular mass compounds (e.g., chloroform and alcohols) and water, which get trapped in some pores and intersegment spaces, thereby preventing the passage of gas. In this regard, the accurate selection of polymers (in terms of structure, solvent, and dry time) in the membrane can influence the degree of success in enhancing the efficiency of O_2/N_2 separation [18]. Before continuing the introduction, it is important to define permeability and selectivity parameters in gas separation applications. Bernardo et al. [17] defined permeability as the rate at which any compound permeates through a membrane, depending upon thermodynamics (partitioning of species between feed and membrane phases) and kinetics (diffusion in a dense membrane or surface diffusion in a microporous membrane). For membranes with varying thicknesses, permeance is used instead of permeability, which is dependent on permeability and thickness [19].

The selectivity is defined as the ability of a membrane to completely perform a separation process (involving the membrane's relative permeability for feed species), allowing for the achievement of high purity of product at high recoveries [17]. The selectivity is affected by the feed composition, flow rate, flow configuration, pressure, and temperature [20]. The results of a database with 1672 records for more than 280 different membranes indicated that most of the attributes (e.g., thickness of the film, pore size, pressure, and temperature) had an insignificant linear correlation with gas permeability, proposing it as a specific and complex relationship. The total volume of the pores, micropore volume, and BET area were found to be the morphological attributes, having a linear correlation with gas permeability and being good indicators of the performance of different kinds of polymeric membranes [21].

Gas separation follows three steps: the permeant sorption into the membrane, permeation induced by diffusion, and desorption occurring at the membrane's low-pressure side. In general, polymer membranes suffer from a trade-off between permeability and selectivity, indicating that these two parameters are antagonistic, as described by Robeson.

Adding a filler to the membrane gives a chance for the texture of the polymer to improve permeability, selectivity or both of them, which act as the key separation parameters. Dispersing fillers in the polymer matrix can help improve gas separation factors with minimal sacrifice in processability and cost [21,22]. In this way, MMMs are defined as the incorporation of solid particles into a continuous polymer matrix [23]. The realization of suitable adhesion and incorporation between polymers and inorganic fillers is the first step to achieve an efficient membrane. It should be noted that the contact position between polymers and solid particles must be void of any gap, thereby preventing the blockage of access to the surface of particles [23].

Non-ideal effects of inorganic fillers dispersed in polymers include undesirable voids or interstitial spaces in the interface of solid particles and texture of polymers, forming varying degrees of rigidification in the surrounding polymer, and creating partial or apparent clogging of polymer along with dispersed segments [22]. Also, dispersing fillers decreases mechanical resistance and causes accumulation in the surface of the polymer. Some studies of magnetic membranes have also highlighted the role of polymer solvents in the separation process [24,25]. The small difference between kinetic diameters of oxygen (r = 3.46 Å) and nitrogen (r = 3.64 Å) makes the separation process cumbersome and time-consuming using the molecular sieve method [24,25]. The O_2 molecule is paramagnetic with the magnetic moment of $\mu_{o2} = 2.95\ \mu B = 2.73 \times 10{-}23\ J\ T^{-1}$, whereas N_2 molecule is diamagnetic [24,25].

This significant difference between magnetic properties of O_2 and N_2 molecules proposes a way to separate them from each other. In a recent study, combining different magnetic particles (having ferromagnetic, ferrimagnetic and superparamagnetic properties) with a variety of polymers has attracted the attention of researchers. In this case, the problem of accumulation of magnetic particles could be solved by applying an external magnetic field to the membranes. However, it may be challenging to create uniform distributions of magnetic particles at the boundary of membranes. In other words, due to the presence and orientation of magnetic domains, the concentration of particles in the boundary is high, which is considered a disadvantage. The use of magnetic fillers and magnetic fields in the fabrication and during the gas testing processes can provide tunable separation properties for the membranes.

One of the noticeable features of magnetic membranes is the formation of magnetic channels, which can be activated by an external magnetic field and enhance the separation efficiency. This issue will be further addressed in this review. The studies carried out in the literature

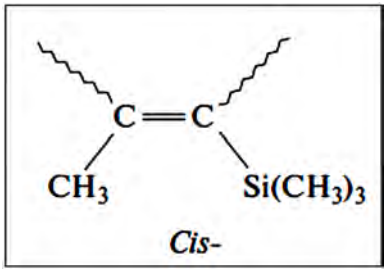

Fig. 1. *Cis*-isomer of the elementary unit of PTMSP. Reprinted from Ref. [50], Copyright(2020),with permission from Springer.

indicated that magnetic channels can act as an absorber of oxygen and be repulsive to nitrogen. The performance of MMMs can be changed depending on nonporous and porous fillers. Nonporous fillers modify the polymer texture to transport the gas through the MMM [16]. On the contrary, the size and shape of the pores of inorganic fillers play an important role in the gas separation performance, making it necessary to consider the adsorption and sieve mechanism. Therefore, the interaction between the polymer and the filler, as well as the gas molecular properties, can influence the separation performance of MMMs with nonporous and porous fillers.

The permeability of membranes is governed by the diffusivity and solubility through the solution-diffusion method, whereas the selectivity is more effective in determining the gas separation. Accordingly, adding solid particles in the polymer texture improves both the selectivity and permeability parameters. Notably, zeolite particles, metal organic frameworks, ZIFs, carbon nanotubes (CNTs), titanosilicate, silica, TiO_2, cobalt phthalocyanine microparticles, zirconium-chromium metals, para-phenylenediamine, barium ferrite, and iron oxide (Fe_3O_4) have been used as fillers in polymeric membranes to improve gas separation properties.

In this review, we present and discuss different structures and properties of pure and particle-mixed polymers for O_2/N_2 gas separation. The results of studies on the use of polymers and fillers in the membrane separation performance are presented in order to find the optimum conditions. We focus on advantages and obstacles of using magnetic materials in the membrane fabrication. The problem of particle accumulation in the boundaries due to drift and orientation of magnetic particles in the polymeric texture is further discussed using field-emission scanning electron microscopy (FE-SEM). Finally, basic concepts of magnetism in polymer membranes such as magnetic domains, coercivity, magnetic channels, and external magnetic field effects are highlighted. This review proposes the role of magnetic materials, magnetic module, and magnetic field as three effective factors to increase the efficiency of magnetic membranes in separation of O_2/N_2.

2. Polymeric membranes

2.1. Polyimide (PI) membranes

The preparation and O_2/N_2 gas separation investigation of amorphous amino-modified silica nanoparticles (AAMSN)/polyimide (PI) membrane have been reported by Hu et al. [26]. Although the permeability of O_2 (at a pressure of 2 atm and temperature of 35 °C) decreased from 10.5 Barrer for PI membrane to 8.5 Barrer for AAMSN (3 wt%)/PI, increasing the AAMSN content to 20 wt% significantly enhanced the O_2 permeability to 29.5 Barrer. Nevertheless, no changes were observed in O_2/N_2 selectivity [26]. Feng et al. [27] studied the effect of thermal annealing on gas separation parameters of block PI membranes. They found that increasing the annealing temperature from 150 to 250 °C can enhance the average interchain distance, thus increasing the permeability in two types of 6FDA-DETDA/DMMDA membranes (having different 6FDA-DETDA block lengths). Also, they indicated that the damaging of imide rings by thermal cross-linking of free radicals at 350 °C and recoveries of imide rings in the cooling process might cause

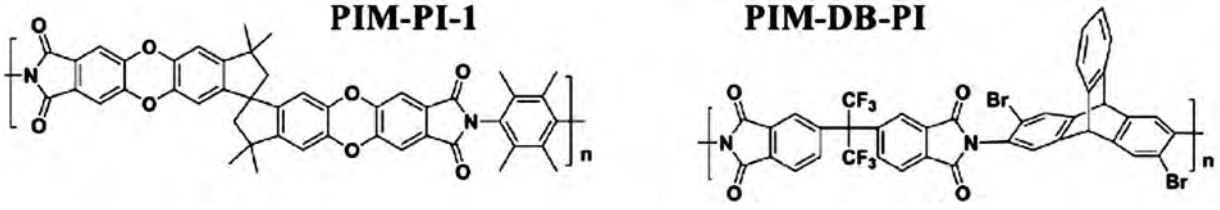

Fig. 2. Resonance structures of PIM-PI-1 (left) and PIM-DB-PI (right) polymers. Reprinted from Ref. [63], Copyright (2021), with permission from Elsevier.

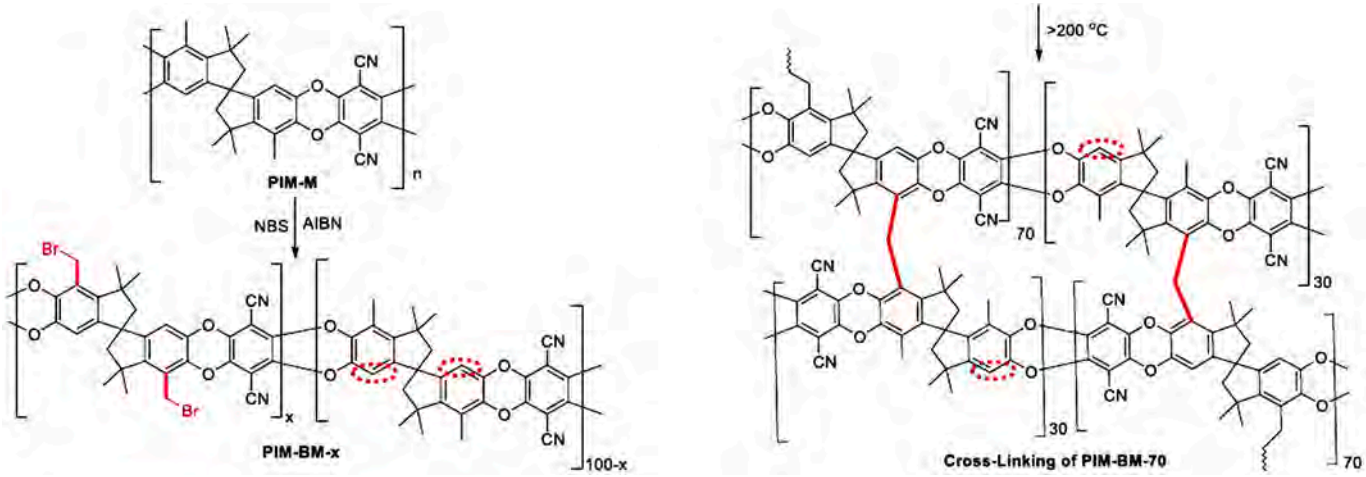

Fig. 3. Resonance structure and synthetic route of PIM-BM-x (left) and self-cross-linking of PIM-BM-70 (right). Reprinted from Ref. [64] Copyright (2020), with permission from ACS.

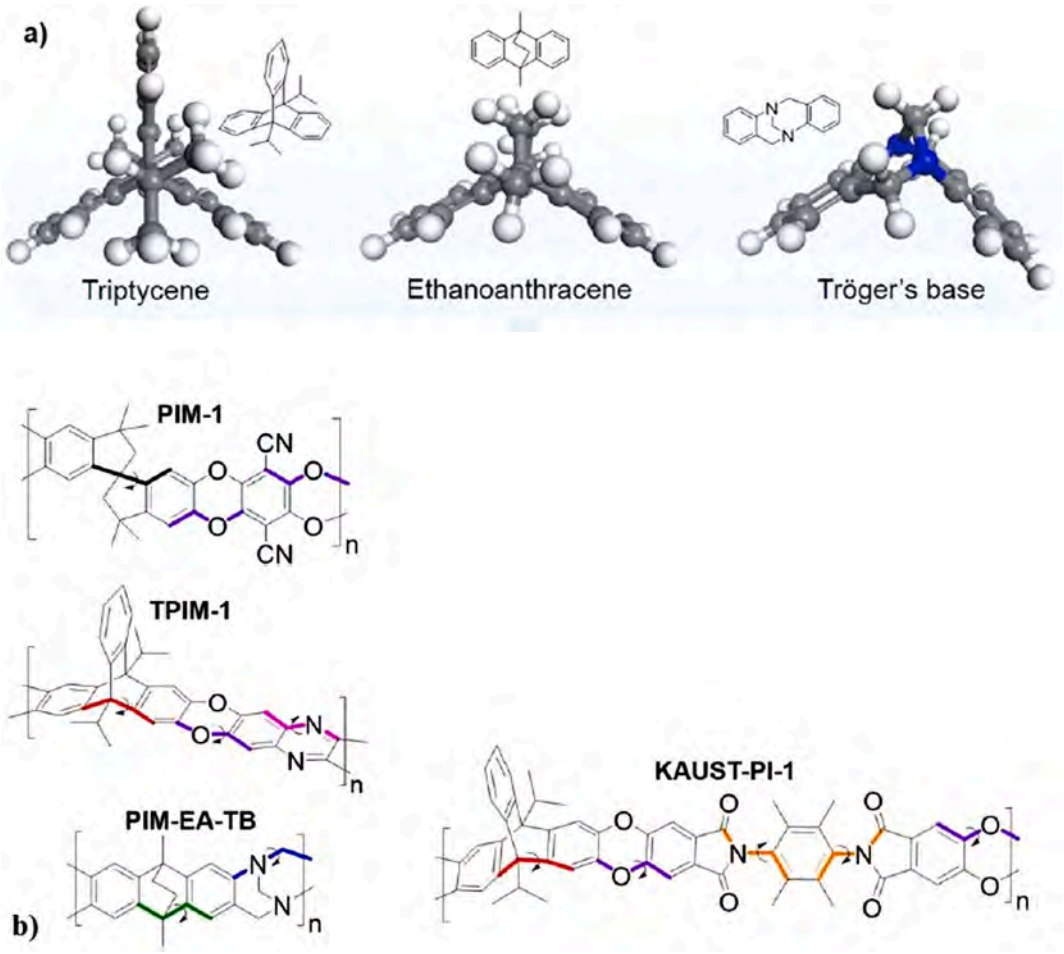

Fig. 4. (a) The core bridged-bicyclic building blocks of intrinsically ultramicroporous PIMs. Reprinted from Ref. [70] Copyright (2015), with permission from ACS. (b) Resonance structures of PIM-1, TPIM-1, PIM-EA-TB (ladder polymer), and KAUST-PI-1 (semiladder polymer). The TPIM-1 has a more rigid backbone and initially higher FV of PIM-1. Reprinted from Ref. [69], under a Creative Commons CC-BY-NC-ND license.

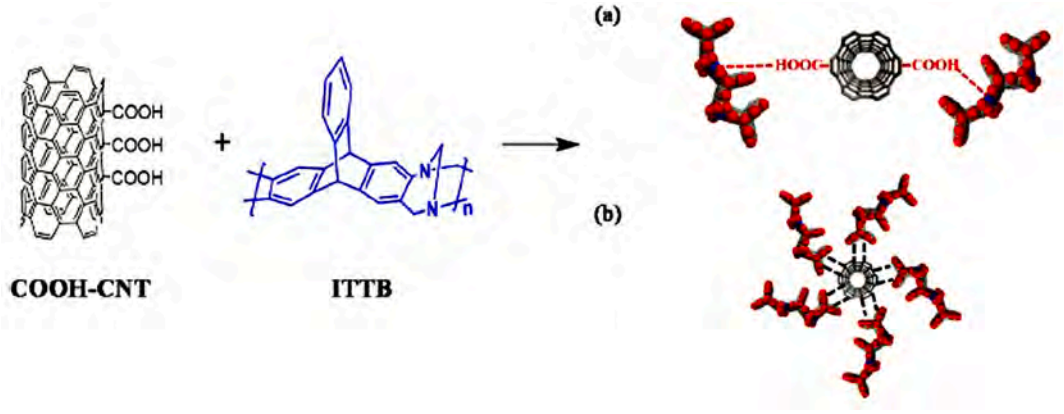

Fig. 5. Schematic representations of: (a) Lewis acid-based interaction between COOH and TB, and (b) π-π interaction between CNT skeleton and triptycene unit. Reprinted from Ref. [71], Copyright (2021), with permission from Elsevier.

the rearrangement of the microstructure and facilitate the gas transition [27].

Escoriala et al. prepared a series of an aromatic PI (6FDA-6FpDA) and blends of copolyetherimides and PIs (6FDA-6FpDA-PEO2000+6FDA-6FpDA) with different polyethylene oxide (PEO) ratios. By increasing the PEO content in non-treated membranes, phase segregation was minimized due to the PEO chains exceeding the FV, thereby decreasing the gas permeability. Thermal treatment of the membranes was also carried in air at 290 °C or in N_2 at 390 °C. In this case, the thermal treatment in N_2 at 390 °C showed higher permeability than that in air at 290 °C, arising from creation of stronger crosslinking reactions in the more oxidizing atmosphere [28]. By introducing isophthalic dihydrazide (IPD) molecules as cross-linkers into 6FDA-durene polyimide (Du-PI) membranes, hydrogen bonding was formed between Du-PI and IPD, and modified the polymer interchain interaction and interchain spacing without destroying the chemical structure of PI,

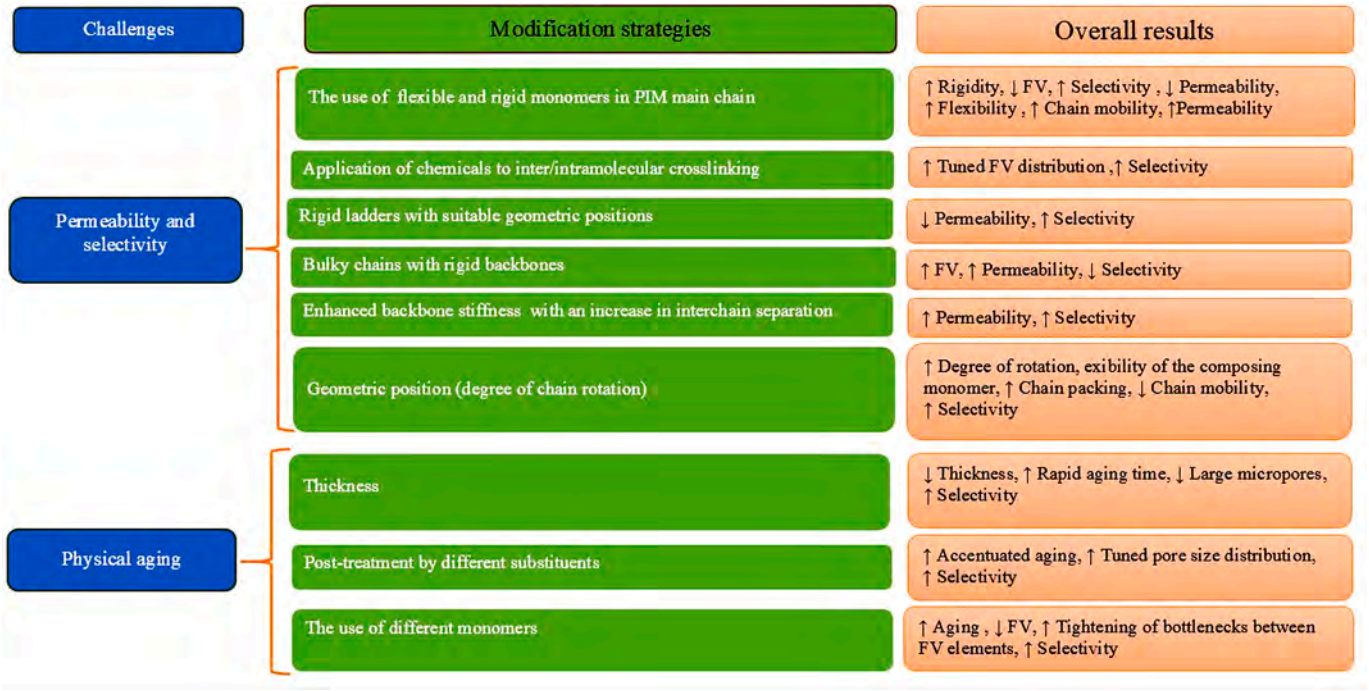

Fig. 6. Modification strategies and overall results of O_2/N_2 separation properties in the case of PIM polymeric membranes.

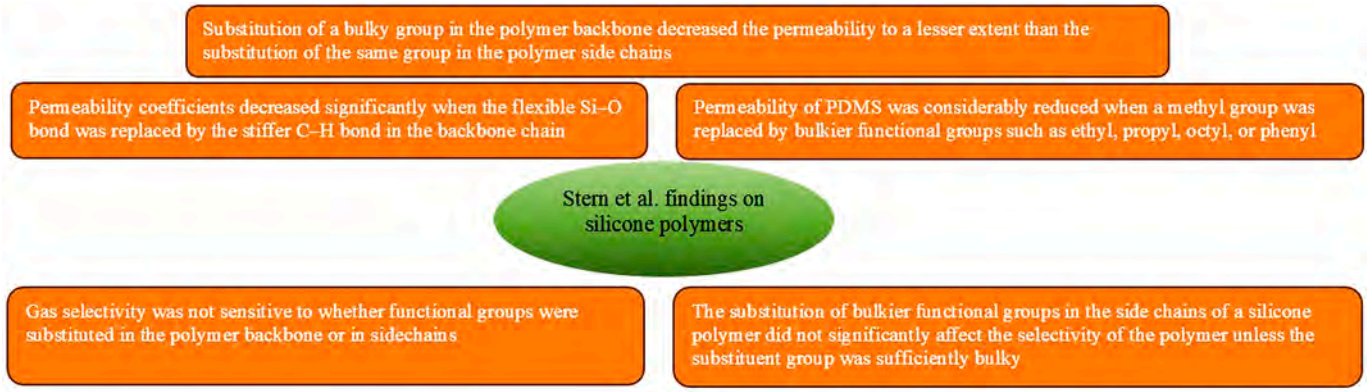

Fig. 7. The summary of the findings on O_2/N_2 separation properties of silicone polymers by Stern et al. [78].

while also increasing the packing density of polymer chains. Thus, O_2/N_2 selectivity increased by 66 % in IPD (20 wt%)/Du-PI membranes [29].

Alvarez et al. studied a series of new diamine monomers (9,9-bis(4-amino-3,5-dimethylphenyl) fluorene (TMCardo) and 3,3′,5,5′-tetra-methyl-4,4′-bis(4-amino-2-(trifluoromethyl)phenoxy)-1,10-biphenyl (CF3TMBP). The effects of introducing two dianhydrides (a very rigid pyromellitic dianhydride (PMDA)) and a more flexible 2,2-bis(3,4 dicarboxyphenyl) hexafluoropropane dianhydride (6FDA) into the polymer backbone were investigated in order to reach high fractional free volume (FFV) and gas separation factors in PI membranes. In this series of membranes, PMDA-CF3TBAPB showed maximum permeability values of 90 and 26 Barrer for O_2 and N_2, along with the highest O_2/N_2 selectivity of 5.7 for 6FDA-Spiro membrane. Moreover, PMDA-CF3TBAPB showed higher intermolecular distances, thus creating a larger size of FV elements [30].

In another study, Park et al. [31] synthesized a series of semi-alicyclic aromatic PIs using 5-(2,5 dioxotetrahydrofuryl)-3-methyl-3cyclohexene 1,2 dicarboxylic anhydride (DOCDA) and five aromatic diamines (pPDA, pDPDA, BAPF, MDA, and ODA) with different chemical structures. They reported higher permeability (2.2 and 1.69 Barrer for O_2, and 0.66 and 0.61 Barrer for N_2) and lower O_2/N_2 selectivity (5 and 5.5) for DOCDA-pDPDA and DOCDA-BAPF membranes.

The DOCDA-ODA membrane showed the highest ideal selectivity (6.5) of O_2/N_2 [31]. Wang et al. [32] studied a series of dual cross-linkable PIs derived from 4,4′-diamino-2,2′-biphenyldicarboxylic acid (DCB) containing two carboxyl groups (4,4′-hexafluoroisopropylidene) diphthalic anhydride (6FDA), 2,4,6-trimethyl-1,3-diaminobenzene (DAM), and 2,2′-bis(trifluoromethyl)-4,4′-biphenyldiamine (TFMB), which were treated by controlling heating/cooling procedures in a tube furnace to achieve an ultra-micropore membrane. In fact, due to the decarboxylation process and collapse of chain segments in crosslinking system during the thermal treatment, an ultra-micropore membrane with pore size of 2.0–6.0 Å was formed. In this case, the highest permeability (37 Barrer for O_2 and 8.38 Barrer for N_2) was obtained for 6FDA-$DAM_{0.7}$-$TFMB_{0.1}$-$DCB_{0.2}$ membrane heat treated at 400 °C [32].

Fig. 8. Forms of ZIF-7 (ZIF-7-I- and ZIF-7-II-based composites) in the fabrication of MMMs for O_2/N_2 separation. Reprinted from Ref. [79], under a Creative Commons CC-BY-NC-ND license.

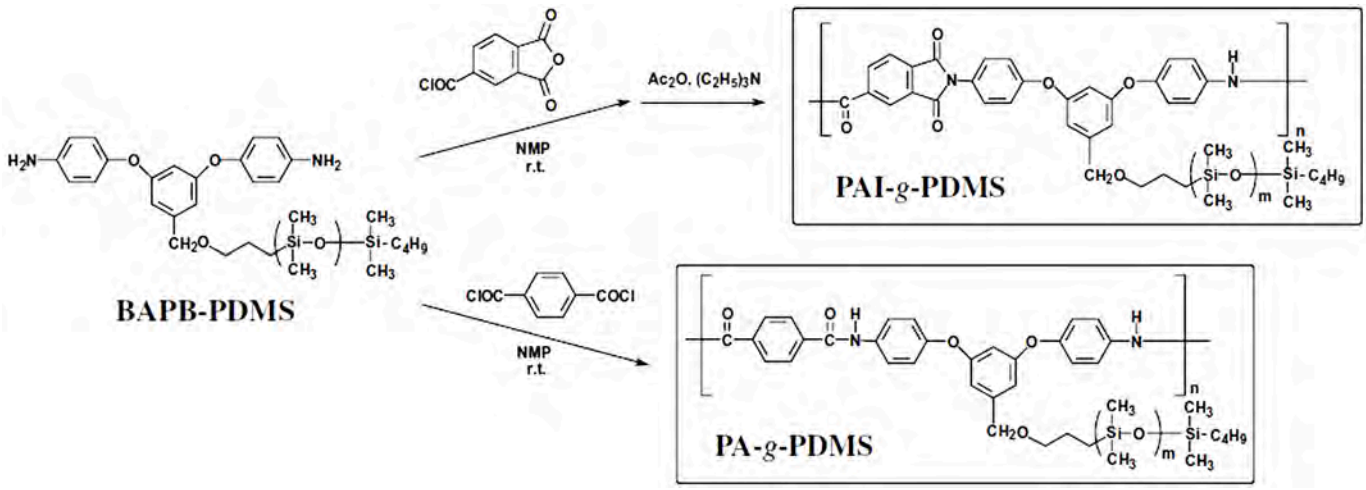

Fig. 9. Resonance structures of PDMS-grafted PAI and PA obtained from the macromonomer BAPB-PDMS. Reprinted from Ref. [86], Copyright (2007), with permission from Elsevier.

2.2. Cardo PI membranes

Cardo PI/TiO_2 MMMs were fabricated using BAPF (9,9′-bis(4-aminophenyl) fluorine) to BTDA (3,3′,4,4′-benzophenone-tetracarboxylic dianhydride) molar ratio of 0.15:1, 4,4′-biamino-3,3′-dimethyldiphenylmethane (DMMDA), and 24 wt% TiO_2 nanoparticles. Poor compatibility between the polymer chains and TiO_2 nanoparticles led to the formation of nano-gaps surrounding the nanoparticles. The aggregation of nano-gaps can create nano-channels like highways that increase the permeance of small molecules (e.g., O_2) and O_2/N_2 selectivity. Therefore, the addition of BAPF and TiO_2 nanoparticles into PI(BTDA–DMMDA) membrane enhanced O_2 permeance and O_2/N_2 selectivity to 4.5 Barrer and 15.8, respectively, being 9.4 and 4.6 times higher than those for pure PI(BTDA–DMMDA) membrane [33]. Zhang [34] fabricated three 6FDA-based PI membranes (6FDA FBPF, 6FDA BPF, and 6FDA MBPF) by using bis(phenyl)fluorine-based cardo diamine monomers with different side groups (–CF3, –H, and –CH3). Due to ineffective chain packing induced by the incorporation of bi(phenyl)fluorene cardo moiety and introduction of bulky CF3 side groups into the PI backbones, O_2 and N_2 permeability improved for 6FDA-FBPF (5.20 and 20.00 Barrer) compared to 6FDA-BPF (1.26 and 4.88 Barrer) and 6FDA-MBPF (0.73 and 3.62 Barrer). In the case of bis(phenyl)fluorine-based cardo PI

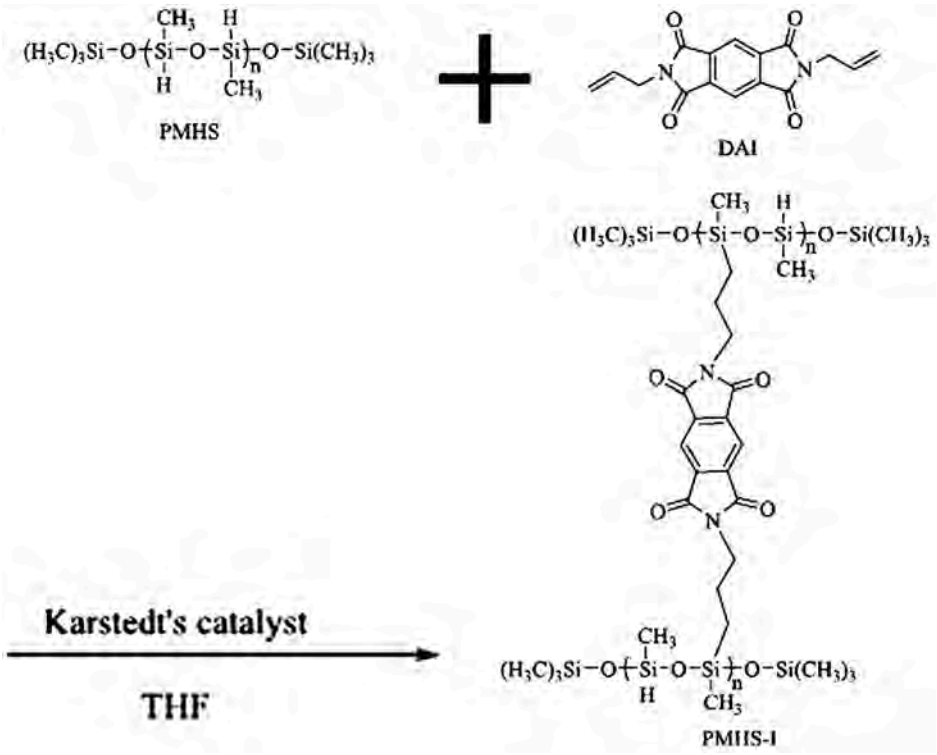

Fig. 10. Synthesis procedure of imido-bridged polysiloxane (PMHS-I). Reprinted from Ref. [92], under a Creative Commons CC-BY-NC-ND 4.0.

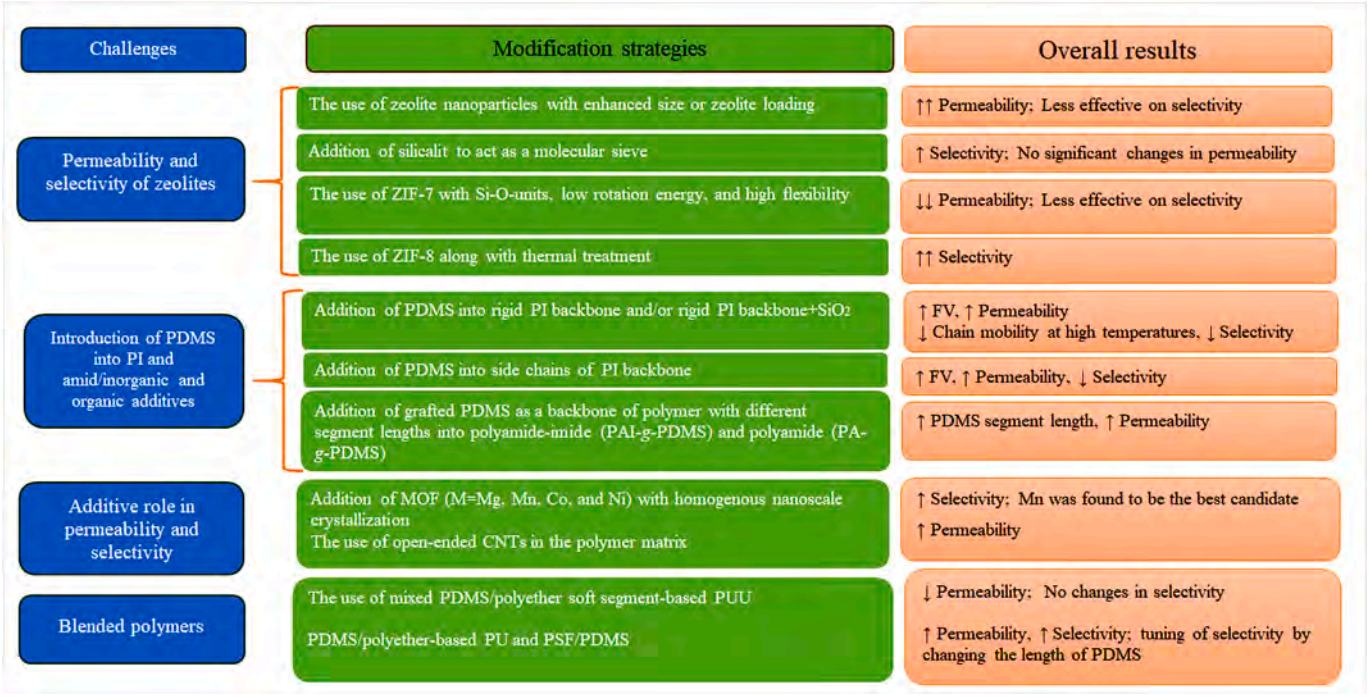

Fig. 11. Modification strategies and overall results of O_2/N_2 separation properties in the case of PDMS polymeric membranes. ↑↑ and ↓↓ are indicative of significant increase and decrease, respectively.

membranes, the highest ideal O_2/N_2 selectivity was measured to be 4.94 for 6FDA-MBPF [34].

Zhang et al. [35] proposed the two following phenolphthalein-based cardo diamines: 3,3-bis[4-(4-amino-3-methylphenoxy) phenyl]phthalide (MPP) and 3,3-bis[4-(4-aminophenoxy)phenyl]phthalide (PP) in order to prepare 6FDA-MPP and 6FDA-PP PIs. They found that *d*-spacing of the PIs increased because of the decomposition of the lactone ring and thermal oxidative crosslinking that enhanced the permeability coefficient. Therefore, highest O_2 and N_2 permeability values were achieved to be 42.2 and 10.6 Barrer for 6FDA-MPP thermally treated at 400 °C, respectively. The best result of the ideal selectivity was about 5.30 for both 6FDA-MPP and 6FDA-PP [35]. The thermal oxidative treatment

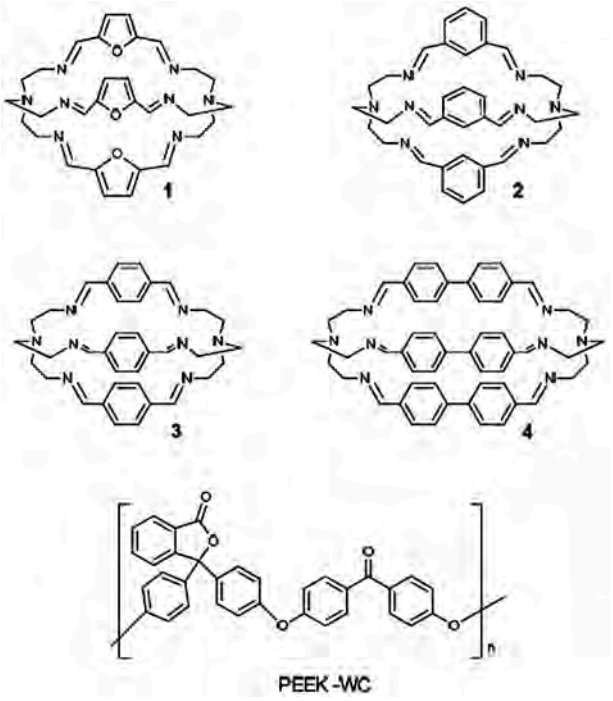

Fig. 12. Resonance structures of four cages (1 = furanyl, 2 = *m*-xylyl, 3 = *p*-xylyl, and 4 = diphenyl) and PEEK-WC polymer. Reprinted from Ref. [161], under a Creative Commons CC-BY-NC-ND license.

was performed to adjust the microstructures and prevent the excessive oxidation of the polymer molecules [35,36].

6FDA-FDA-BisAHPF copoly(amic acid) (PAA) has been synthesized from diamines 9,9-bis(4 aminophenyl)fluorene (FDA), BisAHPF and aromatic dianhydride 2,2-bis(3,4-dicarboxyphenyl) 6FDA, and recovered by thermal treatment under air and N_2 atmosphere in a temperature range between 300 and 480 °C in order to reach thermal oxidative and thermally rearranged (TR) membranes [36]. In the case of thermal oxidative membranes with a thermal treatment temperature of 420 °C, O_2 and N_2 permeability values were obtained to be 99.32 and 15.15 Barrer, respectively, together with O_2/N_2 selectivity of 6.56. In the case of TR membranes thermally treated at 450 °C, O_2 permeability, N_2 permeability and O_2/N_2 selectivity were reported to be 229.03 Barrer, 53.26 Barrer and 4.30, respectively [36]. Zhang et al. prepared PI/nano-attapulgite (ATP) composite membranes by in-situ polymerization of ATP functionalized with a silane coupling agent (KH-550). Although they found no changes in the gas selectivity, the respective permeability of N_2 and O_2 was observed to be 0.13 and 0.84 Barrer, outperforming pure PI membranes [37]. Elsewhere, by incorporation of 0.2 wt% ATP in the PI matrix, the O_2 permeability and O_2/N_2 selectivity increased to 384.5 Barrer and 5.0, respectively [38].

2.3. Poly(1-trimethylsilyl-1-propyne) (PTMSP) membranes

PTMSP is white, amorphic, electrically insulating and soluble, possessing air stability and high thermal stability. This polymer is dissolved in nonpolar solvents such as toluene, cyclohexane, and carbon tetrachloride [39,40]. PTMSP is known as a high-molecular-weight polymer with fairly rigid structure due to its main chain, comprising alternating double bonds and two substituents in each unit [39,41]. The nuclear magnetic resonance analysis of PTMSP membrane indicated that the polymer had only one structure [42]. Irrespective of being glassy at room temperature [43,44], PTMSP has shown large gas permeability in the large scale order of 8800 and 6400 Barrer for O_2 and N_2 gases, respectively [40,44]. In this regard, Srinivasan et al. indicated that fast diffusion (without high solubility) is responsible for the large gas permeability of PTMSP [45].

Table 1
PSF polymers with different additives for O_2/N_2 separation properties.

Polymer	Additive	Description	Ref.
PSF	–	O_2/N_2 selectivity of the skin, substructure, and composite was measured to be 4.7, 0.9 and 4.7 under a feed pressure of 70 psig, respectively.	[93]
PSF	SWNTs	PSF-functionalized SWNT membranes did not show promising results in O_2/N_2 separation.	[94]
PSF	MWCNTs and rGO	The highest permeability was reported for PSF/CNTs/rGO aligned using an AC electric field (O_2 and N_2 permeability of 722 and 301 cc/m^2 day, respectively, along with O_2/N_2 selectivity of 2.39). The physical hybridization of graphene layers and MWCNTs in the composite membrane showed greater permeability as well as better selectivity (O_2/N_2 selectivity of PSF/MWCNTs and PSF/rGO was reported to be 4.73 and 5.39, respectively).	[95]
PSF	Silica	For PSF/silica (20 vol%), O_2 permeability increased up to 380 %, whereas the O_2/N_2 selectivity decreased by 80 %.	[96]
PSF	ZIF-7	The guest-free ZIF-7-I nanocrystals mixed in PSF texture indicated good results for O_2/N_2 separation. The suitable crystallographic pore size was ~3.0 Å.	[79]
PSF	ZIF-95	Loading of 24 wt% of ZIF-95 was the best choice to improve O_2 permeability and O_2/N_2 selectivity by 78 % and 15 % compared to pure PSF membrane.	[97]
PSF	CMS	The selectivity increased from 5.50 in net membrane to 5.97.	[98]
PSF	6FPSF + TMS	O_2/N_2 selectivity was moderately declined, whereas O_2 permeability increased significantly from 3.4 to 18 Barrer to 28 and 23 Barrer for 6FPSf-TMS and TM6FPSf-*s*-TMS, respectively.	[99]
PSF	ZIF-67	Ideal selectivity of 6 wt% ZIF-67 in PSF/ZIF-67 outperformed at a low pressure.	[100]
PSF	Zeolite A nanocrystals	By adding 25 wt% zeolite nanocrystal, O_2/N_2 selectivity and O_2 permeability improved from 5.9 to 7.7, and from 1.3 to 1.8 Barrer, respectively.	[101]
PSF	Cloisites15A	O_2/N_2 selectivity (6.74 for PSF/C15A$_1$) was enhanced more than 24 % compared to the neat membrane. PSF/P–C15A (1 wt%) MMMs exhibited 274 % increase in O_2 gas permeability.	[102]
PSF	Siliceous MCM-41 molecular sieve	O_2 permeability increased from 1.5 to 3.83 Barrer, and N_2 permeability increased from 0.257 to 0.753 Barrer. The ideal selectivity remained almost constant.	[103]

As pointed out by Stern et al., the excess of FV may be responsible for the large diffusivity of gases in polymers, leading to the formation of a large space between polymer segments by the bulky chains of trimethylsilyl group [41,46]. Since the polymer chains are not firmly attached together, preexisting gaps or microvoids form between them, being indicative of the microporous structure of the polymer [44]. On the other hand, the fast diffusion forming the microvoids was linked between the chains with a width of 3 Å. Also, low sorption indicated the large size of microporoes [44]. It has been found that the permeability increases in PTMSP by increasing temperature. Unlike the permeability, the value of selectivity is somewhat smaller [43]. The activation energy for permeability (E_p) of PTMSP is extraordinarily small and negative compared to other polymers, which refers to a lower temperature and thus higher permeability [43]. A negative value of E_P shows that the

Table 2
PSF polymer blends for O_2/N_2 separation properties.

Polymer blend	Description	Ref.
PSF/PI	By decreasing PSF content in PSF/PI, O_2 permeability decreased. PSF/PI (20/80 wt%) showed minimum O_2 permeability, whereas maximum N_2 permeability was obtained for PSF/PI (80/20 wt%).	[104]
PES/PSF (80/20 wt%) blend + zeolite 4A	PES/PSF (80/20 %) + more than 30 wt% zeolite 4A increased the permeability of O_2, whereas N_2 permeability decreased rapidly because of the agglomeration of nanoparticles. The selectivity improved by loading of zeolite 4A up to 25 and 30 wt%.	[105]
Surface modified macromolecules/PSF (SMM/PSF)	SMMs/PSF was immersed in isopropanol non-solvent instead of water, demonstrating stronger affinity to the polymer for 10, 20, 60, and 90 s. O_2 permeance decreased and O_2/N_2 ideal selectivity increased with an increase in the immersion time. The nSMM-blended membrane did not have good performance because of non-selectivity toward oxygen and nitrogen. cSMM-PPG and cSMM-PEG increased the selectivity by increasing the skin selective layer's thickness and preventing the creation of defective pores.	[106]
Composite polymers of PSF family		
Tetramethyl bisphenol A polysulphone (TMPSF) Dimethyl bisphenol A polysulphone (DMPSF) Dimethyl bisphenol Z polysulphone (DMPSF-Z)	The permeability of TMPSF with open structure was several times more than PSF with similar selectivity (1.4 in PSF and 5.6 in TMPSF for O_2 permeability). The DMPSF, DMPSF-Z with more closed structures led to very high selectivity (from 5.6 in PSF to 7.0 and 7.2 in DMPSF, DMPSF-Z).	[107]
Polysulfone copolymers: tetramethyl naphthalene polysulfone (TM-NPSF) Hexafluoro naphthalene polysulfone (HF-NPSF) Tetramethyl hexafluoro naphthalene polysulfone (TMHF-NPSF)	O_2/N_2 selectivity of aromatic polysulfone copolymers TM-NPSF, HF-NPSF and TMHF-NPSF at 2 atm was reported to be 7.58, 6.62 and 5.67, respectively, being much higher than that of commercial PSF.	[108]
Tetramethyl biphenol polysulfone (TMBIPSF) Hexamethyl biphenol polysulfone (HMBIPSF)	The polysulfones with methyl ring substitutions (TMBIPSF and HMBIPSF), BIPSF, and PSF had the same permeability (~1.4 Barrer) and selectivity (~5.6). Although tetramethyl substitution of biphenyl rings increased O_2 permeability from 1.4 in PSF to 5.6 and 5.8 in TMPSF and TMBIPSF, hexamethyl substitution did not significantly change the separation parameters.	[109]

transition of gas through the polymer occurs due to an activated diffusion process [46]. The PTMSP was limited to be used in industry due to its high solubility in hydrocarbon solvent [47].

2.3.1. Modification of PTMSP membrane by adding organic, inorganic, and cross-linker materials

The addition of 3.4 wt% dioctyl phthalate to PTMSP membrane caused permeability to be reduced. Meanwhile, O_2/N_2 selectivity improved to 3.3, starting from 1.6 for pure PTMSP membrane. Nakawa et al. observed a remarkable improvement in permeability of PTMSP membrane by adding perfluorotributylamine [46]. PTMSP membrane

Table 3
PES polymers with different additives for O_2/N_2 separation properties.

Polymer	Additive	Description	Ref.
PES	Zeolite (4A, 13X)	O_2/N_2 selectivity increased from 3.71 in PES to 4.40 in PES-4A 50 wt%. Meanwhile, O_2 permeability increased from 0.52 to 1.10 Barrer.	[110]
PES	Zeolite 3A-4A–5A	The gas separation of PES-zeolite 5A membrane considerably outperformed that of PES-zeolite 4A and PES-zeolite 3A.	[111]
PES	Zeolite 3A–4A with aminopropyl)-diethoxymethyl silane (APDEMS)	The maximum percentage of O_2/N_2 selectivity of PES–zeolite 4A-NH_2 and PES–zeolite 5A-NH_2 was approximately 32 % and 22 %, respectively.	[112]
PES	(MIL)-100(Al)	O_2 permeability improved from 213.89 ± 6.81 Barrer in neat PES to 5743.87 ± 27.61 Barrer in 30 % wt.% (MIL)-100(Al). Meanwhile, N_2 permeability was enhanced from 564.52 ± 5.54 to 8536.14 ± 744.06 Barrer.	[113]
PES	Treated zeolite-4A untreated zeolite-4A	O_2/N_2 selectivity and pressure normalized flux observed for O_2 in treated zeolite-4A were 3.3 and 114.7 GPU, respectively. The selectivity of untreated zeolite membrane was 1.67, whereas its pressure normalized flux for O_2 was 9.5 GPU.	[114]
PES	Modified and unmodified CNT	Due to good grafting of PES/modified-CNT, O_2/N_2 selectivity increased from 3.15 in unmodified-CNT to 6.54 in modified-CNT.	[115]
PES	APTES-functionalized MWCNT	O_2/N_2 selectivity and O_2 permeability increased by purification and functionalization of MWCNT using an acid mixture and APTES.	[116]
PES/PI	Zeolite 4A	O_2 permeability of 30 wt% zeolite-loaded was found to be 5.9 and 12.8 Barrer using annealing treatment above and below the glass transition temperature (T_g), respectively.	[117]
PES/PA	PES (as the support layer) and PA (as the selective layer)	Increasing the monomer contact time on the support membrane with a PES concentration of 25 wt% from 2 to 6 min decreased the oxygen permeation.	[118]
PES/PVA, PS and EC	PES/PS PES/PVA PES/EC	18 wt% PES/polyvinylalcohol (PVA) was thicker than PS and EC, resulting in lower permeability and higher selectivity values for PVA composite membranes. Coating 6 wt% of EC solution on 25 wt% of PES created a uniform and compact active layer, thereby improving the selectivity of the composite membrane. PES (≤18 wt%) was not able to produce a membrane with	[119]

(*continued on next page*)

Table 3 (*continued*)

Polymer	Additive	Description	Ref.
		the ability to separate oxygen from nitrogen.	
PES-OCH_3 PES-OH PES/TFN, and PES-BZP		Due to larger FFV and lower packing density, the best value of selectivity was 8.44. O_2 and N_2 permeability values were observed to be 0.268 and 0.032 in PES grafted with the trifluoromethyl side group (PES-TFN) membranes, respectively.	[120]
PA6/PES	Polyamide6(PA6)	O_2 permeability was significantly enhanced, thus increasing O_2/N_2 selectivity from 0.98 to 4.86.	[121]
PES	Fluorination of PES	5 min fluorination of PES membrane provided optimum gas separation properties by increasing O_2/N_2 selectivity of 5.7 at a pressure of 5 bar.	[122]
PES	Graphitic carbon nitride ($g\text{-}C_3N_4$) nanosheets	Both of the rigidified polymer chains and the impermeable crystalline regions existing in matrix of polymer caused a decrease in permeability coefficient so that a significant enhancement in the selectivity of PES/$g\text{-}C_3N_4$ MMMs was observed.	[123]
PES	PSF-b- PES-PPI	O_2/N_2 selectivity improved from 3.3 in PSF-b-PES-PPI (5:15)DMAc and 5.2 in PSF-b-PES-PPI(5:15) NMP to 10.6 in PSF-b-PES-PPI(5:15) BA.	[124]

crosslinked with 4,4′-diazidobenzophenone bisazide exhibited an increase in O_2/N_2 selectivity to 3.8. However, no significant changes were observed for the selectivity of PTMSP/nonporous fumed silica and PTMSP/TiO_2 [45].

Golubev et al. fabricated PTMSP membrane containing 3 wt% hyper crosslinked polystyrene. The large FV of hyper crosslinked polystyrene led to an increase in the FV of the composite, thereby enhancing the gas permeability. In this way, the selectivity remained almost unchanged [48]. The study of PTMSP nanocomposite membrane prepared by a sol–gel copolymerization approach with different TEOS/OMDEOS molar ratios (1:0, 1:1, 1:2, and 2:1) and constant silane concentration of 15 wt% (based on polymer content) showed ($\alpha = \frac{P_{O2}}{P_{N2}} = \frac{770}{300}$) for a molar ratio of 1:0 [49].

2.3.2. Role of cis-units, antioxidants and thermal treatment

Matsona et al. [50] prepared PTMSP films with different configurations and concentrations (40–80 wt%) of *cis*-units, as shown in Fig. 1. The corresponding permeability was observed to decrease from 11900 to 7900 Barrer for O_2 and N_2 in 40 wt% cis units of PTMSP TC with cluster size of 18.34 ± 3.18 to 8600 and 5400 Barrer for O_2 and N_2 in 80 wt% cis units of PTMSP NB with cluster size of 6.76 ± 1.62 nm [50].

Makrushin et al. [51,52] studied the aging effect on gas separation parameters in the PTMSP series containing *cis*-units and antioxidant Irganox 1076 (octadecyl β-(3,5-di-tert-butyl-4-hydroxyphenyl)-propionate). They found increased stereoregularity and decreased physical aging rate in the PTMSP series containing 50–90 wt% *cis*-units with an aging time of 1 month in air. Also, they reported a slow-down in the aging rate after the addition of Irganox 1076 to the PTMSP mixture. In this case, the gas permeability of the aged films containing antioxidants was higher than that of pure PTMSP films [51].

Interestingly, different concentrations of *cis*-units led to changes in the packing density of macrochains in the configurational composition

Table 4
PEBAX polymers with different additives for O_2/N_2 separation properties.

Polymer	Additive	Description	Ref.
PEBAX-1657	MWNT cross linked TDI	Increasing FV in the presence of MWNT loaded uncross-linked membranes led to a high flux with low selectivity. The selectivity improved from 2.1 in PEBAX to 7.1 in PEBAX cross linked with TDI.	[125]
PEBAX-1657	Silica	O_2 and N_2 permeability increased from 5.84 to 11.3 Barrer and 1.71 to 3.52 Barrer after adding 2.85 wt% Pebax-3.96 wt% TEOS-27 wt% SiO_2 to neat-Pebax. The range of O_2/N_2 selectivity changed between 3.2 and 3.4.	[126]
PEBAX-1657	CuNi-MOF	The permeability and selectivity of Pebax®1657 did not considerably change upon the addition of CuNi-MOF.	[127]
PEBAX-1657	ST-NaX; surface-treated zeolite	Due to partial pore blocking and polymer chain hardening, a negative effect in the permeability was observed after the modification of NaXNCs. By adding 16.7 wt%. of ST-NaX-NCs, O_2/N_2 selectivity was increased by 204 % compared to the neat PEBAX membrane.	[128]
PEBAX-1657/ PES	NaX zeolite, ZIF-8, SiO_2	The incorporation of NaX zeolite (pore size: 7.4 Å) and ZIF-8 (pore size: 3.4 Å) nano-fillers up to 2 wt % resulted in selectivity of 6.06 and 3.85, respectively. The selectivity of SiO_2 (up to 1 wt%) as a non-porous filler was 3.52. NaX and ZIF-8 possessed suitable interface and uniform distribution in the polymer matrix.	[129]
PEBAX-1657 (active layer)/PES	Nano-zeolite NaX	By using smaller zeolite particles, the area and number of polymer/zeolite interface increased. Thus, the mass transfer resistance increased, and N_2 and O_2 permeability decreased.	[130]
PEBAX-1657	Zeolite 4A	10 wt%. 4A loaded Pebax exhibited optimum results of O_2 permeability (7.8 Barrer), N_2 permeability (1.8 Barrer), and O_2/N_2 selectivity (4.3).	[131]
PEBAX-1657	ZIF-8	FFV of the membrane blended with 3 and 20 wt% of ZIF-8 changed between 0.154 and 0.226. The selectivity was slightly reduced because of non-continuous microvoids in MMM.	[132]
Pebax-1657/ PES	Modified MWCNTs	Due to enhancement in the N_2 permeability with increasing the feed pressure, O_2/N_2 selectivity decreased. By increasing the operating temperature, polymer chains were observed to be more flexible, so that more FV cavities were created, thus facilitating the gas diffusion. The O_2/N_2 selectivity showed a decreasing trend as temperature increased from 30 °C to 50 °C.	[133]
Pebax-1657/ amino-PDMS/PAN	Amino silicone	By increasing Pt complex catalyst concentration, the degree of crosslinking of PDMS increased, thereby enhancing the selectivity of membrane. A high value of selectivity (O_2/	[134]

(*continued on next page*)

Table 4 (*continued*)

Polymer	Additive	Description	Ref.
		$N_2 = 2.1$) was obtained when adding 30 ppm of the catalyst.	
Pebax-1657/ PES	Cobalt(II) phthalocyanine (CoPc)	Due to the facilitated transport of O_2 through the membrane, permeance and selectivity were enhanced. The permeance of O_2 improved from 0.06 to 1.12 GPU, and O_2/N_2 ideal selectivity increased from 2.9 to 8.5 by increasing CoPc loading from 0 to 1 wt% at a constant feed pressure of 2 kg cm^{-2}.	[135]

of polymers, thus determining the level of the FV and its structure (namely, the interconnected FV element size) through which the penetrant gas molecules were transported [50–52]. In order to slow down the physical aging and reduce the chemical aging by removal of active reagents, Golubev et al. introduced hyper-crosslinked polystyrene (HCPS) into the PTMSP, followed by performing a thermal treatment at 100 °C for 300 h. In this regard, the lowest permeability of O_2 and N_2 was observed to be 57 and 52 Barrer using PTMSP/HCPS (5.0 wt%), respectively. The O_2/N_2 ideal selectivity changed in the ranges of 1.6–1.7 and 1.9–2 before and after the thermal treatment, respectively [53].

Kossov et al. investigated the effect of thermal annealing on PTMSP membrane with *cis*-units in the presence of phenolic antioxidants. The annealing process of stabilized PTMSP membrane slightly decreased the permeability, whereas it remained unchanged by further heating. The *cis*-enriched membranes did not show any oxidation or decrease of permeability in the transportation during the heating process at 140 °C for 240 h [54].

2.4. Polymers of intrinsic microporosity (PIMs) and microporous ladder polymers

2.4.1. PIM-based membranes

Carta et al. [55] fabricated PIM-ethanoanthracene (EA)-Tröger's base (TB) and PIM-spirobisindane (SBI)-TB membranes. By introducing TB into the PIMs, an inflexible structural unit was formed. Moreover, in-built amines for quaternization by reaction with alkyl dihalides were proposed, which induced stability and reduced physical aging [55] The resulting O_2/N_2 selectivity was reported to be 4.1 and 3.1 for PIM-EA-TB (181 μm in thickness) and PIM-SBI-TB (157 μm in thickness) membranes, respectively.

The more flexible behavior of SBI than EA component caused molecular sieve behavior of PIM-EA-TB to be enhanced, involving the combined rigidity of the bridged bicyclic TB and EA units rather than originating from the TB unit alone [55]. Bezzu et al. [56] studied PIM membranes fabricated by adding fusing rigid and bulky triptycene (Trip) to the SBI unit (PIM-SBI-Trip) and its copolymer (PIM-1/SBI-Trip), which are well known as ultrapermeable polymers after methanol treatment. The gas separation results indicated that 501-day aged film had lower permeability and higher selectivity compared to the as-fabricated PIM. In other words, O_2 and N_2 permeability values were 6390 and 2315 Barrer for PIM-SBI-Trip, whereas they decreased to 2295 and 471 Barrer after the aging process. Coincidentally, O_2/N_2 selectivity increased from 2.76 to 4.87. This variation behavior was also observed for PIM-1/SBI-Trip and PIM-1 membranes [56].

Ma et al. [57] and Carta et al. [58] studied 100-day aged PIM-TRIP-TB, PIM-TRIP-TB, PIM-EA-TB (181 μm in thickness), and PIM-methanopentacene (MP)-TB (94 μm in thickness) membranes, achieving O_2/N_2 selectivity of 4.3, 5.7, 4.1 and 5.0, respectively. By introducing MP structural unit into the PIM, the separation performance was improved, according to Williams et al. [59]. In this case, molecular

Table 5
PMP or TPX polymers with different additives or treatments for O_2/N_2 separation properties.

Polymer	Additive or treatment	Description	Ref.
TPX	Vinylpyridine irradiation-grafted-TPX	O_2/N_2 selectivity increased from 2.6 in non-grafted-TPX to 11.1 in TPX-g-4-vinylpyridine (88.7 wt% grafting)	[136]
TPX	Al_2O_3	Addition of Al_2O_3 showed better results of O_2 permeability (181.58 Barrer) and N_2 permeability (52.09 Barrer) in comparison with the addition of TiO_2 and ZnO nanoparticles.	[137]
TPX	TiO_2, ZnO, and Al_2O_3	By adding 15 wt% of Al_2O_3 at a pressure of 9 bar, maximum values of O_2 and N_2 permeability were obtained to b 92.5 and 30.0 Barrer, respectively. The best selectivity was 20.6 for 10 wt% of TiO_2 nanoparticles at a pressure of 9 bar.	[138]
TPX		The permeability of semicrystalline poly(4-methyl-1-pentene) (PMP) with $T_g = 30$ °C in the temperature range of −20–80 °C increased exponentially. The O_2/N_2 selectivity decreased from 9.7 at −20 °C to 2.8 at 80 °C.	[139]
TPX	Second bath medium as a treatment	O_2/N_2 selectivity in n-butanol (3.67) was higher than that in methanol (2.66), ethanol (2.95), and n-propanol alcohol (2.85). Storage time decreased the membrane performance. To avoid storage time defects, the membrane was heated at 50 °C for 12 h.	[140]
TPX	Modification by fluorine exposure	The fluorine exposure modified the surface of TPX membrane and increased its selectivity from 3.3 to about 6.5 after 15 min.	[141]
TPX	Homograft treatment	O_2 permeability and O_2/N_2 selectivity for 60 h irradiation using 20 % and 10 % degrees of grafting were 28×10^{-10} cm^3 cm/cm^2 s cm Hg and 7.6, and 63×10^{-10} cm^3 cm/cm^2 s cm Hg and 4.5, respectively.	[142]
TPX	Modification by chlorination	Highly and deeply chlorinated membranes showed decreased permeability of 0.12×10^{-9} cm^3 cm/cm^2 s cmHg. O_2/N_2 separation factor increased from 4.1 in neat TPX to 7.3 in the membranes.	[143]
TPX (MX-001 and RT-18)	Modification by blending of PDMS	By adding 10 wt% of silicone rubber, T_g shifted inwardly and molecular mixing occurred between the silicone rubber and TPX. TPX (MX-001) was more homogeneous and had a lower molecular weight, denser structure and more branching chains than TPX (RT-18). The best result of O_2/N_2 selectivity was 6.92 using 10 wt% siloxane/TPX (MX-001) at a milling temperature of 65 °C.	[144]
TPX/PDMS	Plasma treatment of vinyl monomers	Vinyl monomers were deposited onto blended polymers by plasma, providing a better grafted polymer layer on the surface of the blend membrane.	[145]

(*continued on next page*)

Table 5 (*continued*)

Polymer	Additive or treatment	Description	Ref.
		The best result of selectivity was reported to be about 5.16 for PVAc-p-TPX/PDMS treated by 10W–20 min plasma.	

rigidity was considered the main determinant of intrinsic microporosity and high selectivity.

By maximizing the rigidity of the chains and internal FV of the constituent monomer units, an optimum distribution of small micropores with uniform structure was observed. The results showed an enhancement in O_2/N_2 selectivity from 2.77 for PIM-1 to 6.26 and 6.65 for 118- and 370-day aged PIM-MP-TB, respectively [59].

Aliyev et al. [60] reported O_2/N_2 selectivity of 3.23, 4.30, 4.25, and 4.12 for PIM1, PIM1-4 wt.% TIFSIX3, PIM1-2 wt.% $Zn_2(bim)_4$, and PIM1-8 wt.% MOF-74 membranes, respectively. In the case of PIM-1 and PIM-7 membranes, the respective O_2/N_2 selectivity was reported to be 4 and 4.5. For polymeric gas separation membranes, the backbone stiffness needs be coupled with reasonable increases in interchain separation in order to achieve both higher permeability and selectivity [61]. To obtain inter- and intra-crosslinking reaction sites in PIMs, Li et al. prepared blends of bromomethylated PIM-1 (PIM-BM) and TB as a microporous polymer system. They reported an improvement in O_2/N_2 selectivity from 3.8 to 11.1, together with a reduction in O_2 permeability from 422.5 to 18.2 Barrer for crosslinked PIM-BM/TB treated at 300 °C. The creation of the self-crosslinking within PIM-BM and inter/intramolecular crosslinking (PIM-BM and TB) in polymer blends led to the tuning of FV distribution in crosslinked system, giving rise to the high selectivity [62]. In another study, Xiaohua et al. demonstrated high O_2 permeability (137 and 715 Barrer at −30 °C and 30 °C) and high O_2/N_2 selectivity (10.1 and 6 at −30 °C and 30 °C) using fluorine-functionalized triptycene diamine employed as the building block of Tröger's base-derived polymer (DFTTB) [63,64]. Similarly, Rose et al. [65] reported the synthesis of PIM-BTrip-TB using a polymerization reaction under optimized conditions for the formation of TB by adding monomer 4 to a mixed solution of 5 molar equivalents of dimethoxymethane in the trifluoroacetic acid.

The resulting polymer was found to be highly permeable (3290 Barrer) with moderate O_2/N_2 selectivity of 3.6. Alternatively, the gas separation performance of Br-substituted intrinsic microporous PI (PIM-DB-PI) was compared with that of microporous PIM-PI-1 with more rigidity, showing higher selectivity and lower permeability due to its considerably higher density and lower FFV [63].

It should be noted that, the relatively larger degree of rotation of PIM-DB-PI (508°) compared with that of PIM-PI-1 (315°), as well as the flexibility of the composing monomer in PIM-DB- PI, can lead to more efficient polymer packing, which in turn enhances the selectivity [63]. Fig. 2 shows resonance structures of PIM-PI-1 and PIM-DB-PI polymers.

Chen et al. prepared PIM-BM-x polymers using methylated PIM-M polymers, followed by their bromoalkylation and thermal self-crosslinking reaction (see Fig. 3). The evaluation of separation parameters indicated an improvement in O_2/N_2 selectivity from 3.9 for PIM-M to 5.6 for PIM-BM-100. Also, thermal treatment of PIM BM-70 at 300 °C for 5 h affected the polymer chain packing and decreased *d*-spacing of polymer structure, which enhanced the selectivity from 4.6 to 6.5 [64].

Felemban et al. [65] focused on the reaction of TOT monomer with different bis-catechols in order to prepare high-performance PIMs as membranes (PIM-TOT-100, PIM-TOT-spirobichroman (SBC), PIMCardo-TOT, PIM-TOT-spirobifluorenes (SBF), PIM-TOT-SBF-4, and PIM-TOT-SBF-5) for gas separation applications. While the PIMs treated with MeOH (containing TFTPN units) possessed high permeability, they showed lower selectivity compared to the TOT-based membranes.

By increasing the aging process, FV of PIMs decreased and tightening

Table 6
PU polymers with different additives or treatments for O_2/N_2 separation properties.

Polymer	Additive or treatment	Description	Ref.
PU	SiO_2	O_2 and N_2 permeability decreased from 7.50 to 2.74 Barrer in pure PU to 6.82 and 1.93 Barrer in PU containing 15 wt% of SiO_2 nanoparticles, thereby increasing O_2/N_2 selectivity from 2.75 to 3.65. As the temperature increased, the selectivity decreased from 3.65 at 25 °C to 2.52 at 45 °C.	[146]
PU	Changing hard and soft segment contents	By increasing the hard segment content, FV size and FFV decreased.	[147]
PU [148]	Blending with PMMA	By increasing temperature from 10 °C to 40 °C, FV size increased approximately 30 %, thus increasing permeability of both PU and PU/PMMA blend membranes.	[148]
PU	Blending with polyethylene oxide, polypropylene oxide, and polyethylene oxide triblock copolymer (Pluronic)	O_2/N_2 selectivity of PU (85 wt%)/PVAc (15 wt %)/Pluronic (4 phr) membrane increased 200 %, and its permeability decreased.	[149]
PU	Addition of PMMA	By increasing PMMA content for blends with 80 and 60 wt% of PU, the average FV size of the blends decreased, which was correlated with a decrease in permeability. No significant changes were observed in O_2/N_2 selectivity of PU/PMMA membrane.	[150]
PU	Blending with polysiloxane	Low O_2/N_2 selectivity in the range of 1.3–3.0 was observed. The higher the degree of phase separation, the higher the influence of the soft phase is on the gas permeation. A lower chain packing density increased the permeability.	[151]
PU	Addition of oxygen carrier salt (cosalen)	O_2/N_2 selectivity and O_2 permeability were 8.9 and 1.1 Barrer using PU/5 wt% cosalen at 5 °C, respectively. The gas separation was governed by gas diffusion rather than gas sorption in PU/cosalen membrane.	[152]
PU	Copolymerization (copolyether-urethane-urea, copolyether-urethane)	Phase separation and nature of chain packing with the different extenders in the copolymers affected the separation results. An increase in the packing caused a decrease in the permeability.	[153]
PU	PU/polyether and PU/polyester diols	Due to its less flexible and more stereoregular structure, PU/PE had higher permeability.	[154]
PU	Hybridization of PDMS-PU/POSS nanoparticle	The permeability of N_2 and O_2 in POSS-amine	[155]

(*continued on next page*)

Table 6 (*continued*)

Polymer	Additive or treatment	Description	Ref.
		incorporated hybrid membranes was lower than pure PDMS-PU.	
PU	Amine containing PEG was used as the soft segment component. The hard segment was formed from MDI and chain extended with N-MDEA and/or TEPA.	The PU with 51.5 wt% of the hard segment content had higher O_2 permeability (1.75 Barrer), N_2 permeability (0.374 Barrer), and selectivity (about 4.7).	[156]
PU	DMPA	By increasing 1.5 mol% DMPA content in the composition, the highest O_2/N_2 selectivity (5.1) was obtained.	[157]
PU	SiO_2(polyurethane/silica and polyesterurethane/silica)	Increasing silica nanoparticle loading decreased permeability, whereas it increased O_2/N_2 ideal selectivity. PU100/SiO_2 nanocomposite membranes exhibited higher performance of O_2/N_2 separation (ideal selectivity of PU100/15 wt% SiO_2 was 3.67).	[158]
PU	Boehmite nanoparticles	Permeability of the membrane decreased with increasing the boehmite content, whereas it increased the O_2/N_2 ideal selectivity.	[159]

of the bottlenecks between the FV elements was observed, leading to the selectivity improvement. The O_2/N_2 selectivity of PIM-TOT-SBC, 1028-day aged PIM-TOT-SBC, PIM-Cardo-TOT, 885 day-aged PIM-Cardo-TOT, and 114-day aged PIM-Cardo was reported to be 4.1, 4.3, 4.0, 4.4, and 4.15 respectively [66]. Longo et al. mixed amidoxime-functionalized PIM-1 (AO-PIM-1) and commercial PI Matrimid® 5218, and observed a decreasing trend of permeability due to occupied FV of the AO-PIM-1 after further addition of Matrimid® 5218. The best result of O_2/N_2 selectivity was 6.2 using 80 wt%/20 wt% of Matrimid® 5218/AO-PIM-1 [67]. In fact, the amidoxime modification was selected owing to the tightening of the polymeric matrix and improvement in the selectivity [68].

2.4.2. Microporous ladder polymers

Ma et al. [57] synthesized soluble microporous ladder polymers by combining catalytic arene-norbornene annulation (CANAL) and TBs. They reported O_2/N_2 selectivity of 4.8 and 5.2 for CANAL−TB-1 and 300-day aged CANAL−TB-1 membranes, respectively.

Swaidan et al. studied long-term physical aging and plasticization of ladder and semiladder PIMs polymer families (i.e., PIM-1, TPIM-1, TPIM-2, PIM-EA-TB, and KAUST-PI-1), as depicted in Fig. 4. The results of their study indicated that not only high intrachain rigidities played an important role in physical aging but also the initially high FV induced by larger backbone rigidity and chain architecture acted as a driving force for the fast and more extensive aging process of the bulk microstructure, thereby forming gas separation membranes with high permeability and selectivity. In this way, O_2 permeability of TPIM-1 was reduced by 95 %, whereas its O_2/N_2 selectivity was enhanced by 115 % after an aging time of 780 days [69].

Li et al. reported improved O_2 permeability (701 vs 504 Barrer), selectivity (5.79 vs 5.54), and stability compared to pristine ITTB after adding 1.0 wt% of CNT into TB ladder polymer ITTB. After 100 days of aging, O_2/N_2 selectivity of the CNT-contained TB ladder polymer further increased to 7.28. A good Lewis acid-based interaction between tertiary amine (from TB) and COOH (from CNT), together with π-π interaction between the CNT skeleton and triptycene unit, could be responsible for the selectivity improvement [71]. For better clarity, Fig. 5 schematically shows the aforementioned interactions.

2.4.3. The interplay between aging time and membrane thickness

Some studies performed on the gas separation properties of membranes with different aging time and thicknesses have indicated that physical ageing of polymers, particularly those with high FV, is considerably faster in thin films [72,73]. Furthermore, it has been found that post-treatment by different substituents can affect the aging time [73]. By investigating PIM-SBF series treated by methyl or *t*-butyl substituents, the performance of bulky *t*-butyl groups of PIM-SBF (PIM-SBF-5) was better than that of methyl substituents of PIM-SBFs 2–4 when keeping the distance between polymer chains constant during the aging process. Since the aging preferentially reduced large micropores within the PIM-SBFs, the ideal O_2/N_2 selectivity (2.6) of PIM-SBF-5 with a thickness of 98 μm was lower than that of other PIM-SBFs. Meanwhile, PIM-SBF-1 (80 μm in thickness) showed the highest ideal O_2/N_2 selectivity (5.6) after an aging time of 2088 days [72].

2.4.4. The use of PIMs in the preparation of polymer molecular sieve (PMS)

A PMS precursor of partially amidoxime functionalized PIM-1 (PAOPIM-1) with solution processability was mixed with a thermally stable PI matrix (PI–COOH) to form a polymer blending membrane that was subsequently annealed under controlled heating conditions. The self-cross-linking between nitrile and amidoxime groups at 300–400 °C caused PMS to act as a filler in the matrix of polymer with high homogeneous dispersion. The highest O_2/N_2 selectivity was achieved to be 8.5 using 50 wt% filler loading [55]. Fig. 6 summarizes modification strategies and overall results of the separation properties explained in section 2.4 for PIM membranes.

2.5. Polysiloxane hybrid membranes

2.5.1. Silicalite, silicalite-1, and NaX-dimethylsiloxane (PDMS)

By adding zeolite silicalite with different sizes (0.1, 0.4, 0.7, 0.8, 1.5, and 8 μm) into 20 and 40 wt% PDMS MMMs, the performance results were less affected in terms of ideal selectivity. On the other hand, permeability increased at relatively high zeolite loadings or for relatively large particle sizes. Of course, the role of particle size was far more pronounced in the permeability values [74].

Clarizia et al. showed that the addition of silicalite-1 into the PDMS matrix can slightly improve O_2 and N_2 permeability [75]. They found that O_2/N_2 selectivity trend for different concentrations of NaX-PDMS was similar to that for PDMS films, except the corresponding selectivity values were larger for the films depending on the temperature [75]. Duva et al. investigated gas separation properties of silicalit-1/PDMS and EPDM. Although the silicone rubber (PDMS) and ethylene-propylene rubber (EPDM) had non-selective equilibrium sorption properties, adding silicalite-1 to them induced remarkable O_2/N_2 selectivity improvements. In other words, the addition of 37 wt% silicalite-1 to PDMS and 53 wt% silicalite-1 to EPDM improved the corresponding selectivity to 2.7 and 4.7, respectively [76].

Jia et al. reported an increase in O_2/N_2 selectivity from 2.15 to 2.92 by adding 70 wt% silicalite to PDMS. In fact, silicalite can act as a molecular sieve in transition of smaller molecules and hindering of larger molecules [77]. Moreover, Stern et al. investigated O_2/N_2 separation properties of silicone polymers whose findings are summarized in Fig. 7.

2.5.2. ZIF-7

The PDMS includes a sequence of -Si-O-units with high flexibility due to their low rotation energy, avoiding the effective hindering of the phase transition of ZIF-7 (see Fig. 8). The addition of ZIF-7 nanocrystals with a wide pore (ZIF-7-I) to polysulfone (PSF) and Pebax-1657

Table 7
Some other polymer blends with different additives or treatments for O_2/N_2 separation properties.

Polymer blend	Additive or treatment	Description	Ref.
Polyphenylsulfone (PPSU) and polyphenylsulfone containing imidazole group (imPPSU)	Imidazole groups	By introduction of imidazole groups, permeability of O_2 and O_2/N_2 ideal selectivity decreased from 1.423 Barrer and 4.924 in PPSU to 1.163 Barrer and 1.806 in imPPUS40, respectively.	[160]
Poly(ether ether ketone) with cardo group (PEEK-WC)	M-xylyl imine and furanyl imine as an organic cage with cardo group	Permeability decreased and O_2/N_2 selectivity remarkably increased in the presence of m-xy. The respective selectivity and O_2 permeability of PEEK-WC/m-xy were 9.71 and 0.68 Barrer. The respective selectivity and O_2 permeability of PEEK-WC/Fura were 4.49 and 10.1 Barrer (see Fig. 12).	[161]
Poly (ODPA-TMPDA) (ODPA = 4,4′-oxydiphthalic anhydride; TMPDA = 2,4,6-trimethyl-m-phenylenediamine)/Co^{III} acetylacetonate and SNW-1 nanoparticles	A porous organic framework (SNW-1 nanoparticles) and a cobalt-based complex (Co $(acac)_3$)	A synergistic effect of the combination of 10 wt% of SNW-1 and 2 wt% of Co $(acac)_3$ in a polymer matrix simultaneously increased O_2 permeability and O_2/N_2 selectivity up to 33 % and 18 %, respectively. By adding $Co(acac)_3$, matrix of membranes was densified with reduction of the polymer's FV, thereby decreasing O_2 and N_2 diffusivity by 19 % and 22 % respectively.	[162]
Polybutadiene/polycarbonate (PB/PC)	Plasma treatment by using ethylenediamine plasma (70 W for 40 min)	Plasma treatment facilitated surface crosslinking and created a dense top layer on the membrane surface, thus enhancing the size sieving effect so that the selectivity reached above 10.	[163]
Nafion 117 and PC		Dry Nefion (with O_2/N_2 selectivity of 4.15 and O_2 permeability of 1.08) did not have any advantage relative to PC (with O_2/N_2 selectivity of 5.13 and O_2 permeability of 1.48)	[164]
Styrene-butadiene-styrene triblock copolymers	UV photografting without degassing	O_2/N_2 selectivity improved from 3.1 to 5.6 at 278 K, from 3 to 5.3 at 288 K, from 2.8 to 4.7 at 298 K, and from 2.3 to 3.7 at 308 K when increasing the grafting of DMAEMA from 0 to 4.72.	[165]
Six poly(α-amino acid): poly(l-leucine) (PLL), poly(y-methyl Lglutamate) (PMLG), poly(l-methionine) (PMt), poly(y-benzyl-L glutamate) (PBLG), poly(Aie-carbobenzoxy-l-lysine) (PLy-Z), and poly(y-l-glutamic acid) (PG)		The side chains of poly(a-amino acid) membranes played an important role in permeability of gases. The permeability decreased in the following order PLL > PMLG > PMt > PBLG > PLY-Z > PG, from 8.61 to 0.0006 and 1.92 to 0.0001 for O_2 and N_2, respectively. ($P \times 10^{10}$ (cm^3(SPT)-cm/cm^2-sec-cmHg)	[166]
Miscible poly(methyl methacrylate) and styrene/acrylonitrile (SAN) copolymers		Due to stronger interaction in 13.5 wt% of acrylonitrile (AN) relative to 28 wt% of AN in SAN, polyacrylonitrile had better barrier properties compared to polystyrene, leading to higher permeability. The ideal selectivity of 13.5 wt% of AN was lower than that of 28 wt% of AN.	[167]
Three different PMMA forms (i-PMMA, s-PMM, and 50/50 i-PMMA/s-PMMA blend)		The isotactic form had denser packing in the glassy state and lower FV. The permeability of isotactic-PMMA (0.0168 Barrer for O_2, and 0.0014 Barrer for N_2) was lower than that of syndiotactic-PMMA (0.1050 Barrer for O_2, and 0.0130 Barrer for N_2). O_2/N_2 selectivity of i-PMMA was 12.0, being higher than that of the other polymers.	[168]
PC and PMMA	Controlling annealing temperature and time	The immiscible blend morphology changed to interconnected and domain–matrix structures. Permeability of the immiscible blend with a domain–matrix structure was higher than that with an interconnected structure. The miscible blend had the lowest permeability. The ideal selectivity of miscible blends was higher than that of immiscible blends.	[169]
Carbon composite molecular sieving membranes (CMSMs)	Cerium oxide (CeO_2)	CMSMs were prepared on carbonaceous plate supports using PI as a precursor and CeO_2 as a filler. In CMSMs/CeO2 (0.2 wt%), the selectivity reached 16.3 by increasing O_2 concentration to 77.3 %.	[170]
DOCDA-ODA	20 wt% zeolite LTA	O_2/N_2 selectivity of DOCDA-ODA increased by 122.16 % after addition of 20 wt% zeolite LTA	[171]
poly(trialkylsilylethynylphenylacetylene)s (PSEPAs)	PSEPAs with trimethylsilyl(PSEPAMe), triethylsilyl(PSEPA-Et), triisopropylsilyl (PSEPA-iPr), tripropylsilyl(PSEPA-Pr),	Poly(substituted acetylene)s with the insertion of a conjugated acetylene between the benzene ring and the silyl showed ultra-high oxygen permeability of 3.09×10^5 Barrer.	[172]

(*continued on next page*)

Table 7 (*continued*)

Polymer blend	Additive or treatment	Description	Ref.
	tributylsilyl(PSEPA-Bu), and triphenylsilyl (PSEPA-Ph)	The selectivity of PSEPA-Et, PSEPA-Pr, and PSEPA-Bu membranes was 2.10, 2.20, and 1.33, respectively.	
Hyper-coPI membranes	DAMm:TAPAn-6FDA (m:n = 0.5:1–5:1) (DAM0.5:TAPA1-6FDA)	The corresponding selectivity was reported to be 5.58	[173]

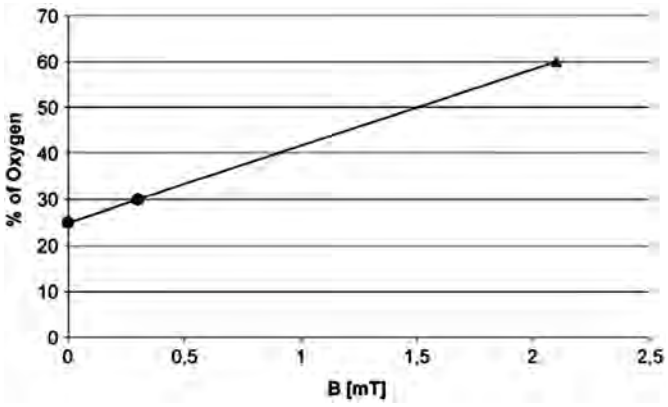

Fig. 13. The variation of oxygen air enrichment as a function of the strength of a magnetic field applied to a membrane filled with neodymium powder (magnetized under a magnetic field of 0.3 mT). Reprinted from Ref. [179], Copyright (2007), with permission from Elsevier.

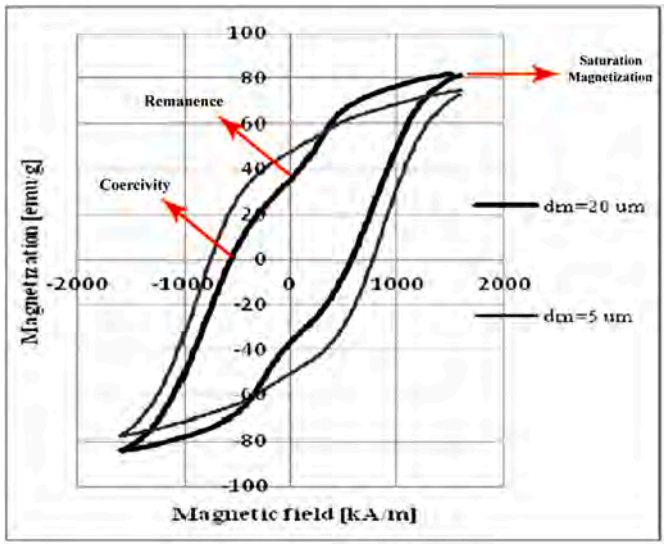

Fig. 14. The comparison between hysteresis loops of magnetic membranes containing particles with two different mean diameters (d_m). Reprinted from Ref. [191],Copyright (2017), with permission from Elsevier.

improved O_2/N_2 selectivity, whereas ZIF-7 with a narrow pore (ZIF-7-II) in PDMS matrix showed a sharp decrease in O_2 permeability and no improvement in O_2/N_2 selectivity [79].

2.5.3. ZIF-8

Dual-layer PDMS/PSF membranes with 2 wt% ZIF-8, 2 wt% NH_2-ZIF-8, and 2 wt% thermally annealed ZIF-8 have been fabricated by Bagri et al. They found that O_2/N_2 selectivity of 2 wt% annealed ZIF-8-membrane was 5.5, outperforming 2 wt% ZIF-8 and 2 wt% NH_2-ZIF-8 membranes with the selectivity of 2.95 and 4.97, respectively [80].

2.5.4. PMA-PDMS-PMA and PMA-PDMS-PMA/PVAc

Semsarzadeh et al. added PVAc to PMA-PDMS-PMA block co-polymers, creating new fibrillar microstructures with improved gas selectivity. The addition of 20 wt% PVAc (as a polar and glassy polymer) increased average fibril diameter of PDMS block copolymer, leading to a 55 % enhancement in the gas selectivity. Due to the polar interaction between -CO-O- groups of PMA and -O-CO- groups of PVAc, the resulting PMA/PVAc had a miscible form [81].

2.5.5. Imide-siloxane block copolymers

By introducing PDMS into a rigid polyimide backbone with a coupling agent in a sol–gel reaction, the gas permeability improved, indicating the occurrence of permeability through the flexible PDMS phase. By adding more silica (SiO_2) in the hybrid membrane, this inorganic additive restricted the thermal chain motion of organic components, thereby retarding the significant reduction of gas selectivity at high temperatures. Although the addition of 0 and 10 wt% silica to the membrane dramatically decreased the selectivity from 8.94 to 8.80 at 30 °C to 3.12 and 4.93 at 100 °C, respectively, 30 and 50 wt% silica added to the membrane slightly changed the corresponding selectivity from 8.71 to 8.00 at 30 °C to 6.21 and 7.10 at 100 °C [82].

Polyamideimide-branched siloxanes (PAIBrSs) membranes were prepared by incorporating ODMS into the side chains of the PAs, providing better gas permeation properties compared to the polymers having ODMS in their main chains. Because of the flexible linkage and free rotation of PAs in ODMS chains, a large distance between the chains was created that increased the FV of the polymer and decreased the O_2/N_2 selectivity [83–85].

The comparison between gas separation results of PAIBrS and poly (imide-siloxane) (PIBlS) membranes caused the selectivity of PAIBrS to be smaller than that of PIBlS membranes [83], which was attributed to the presence of ODMS as side chains in the backbone of poly-amideimid. In another study, the gas permeation of microheterogeneous polymers and the cluster connectivity in pathway of PAs were investigated. Due to formation of shorter paths around the composition (ca. 0.2–0.3 vol fraction of siloxane moiety), the permeability increased and O_2/N_2 selectivity decreased [85]. Ha et al. stated that the gas transport using poly(amide-imide) siloxane copolymers is dominated by the siloxane phase (as a flexible domain) and the poly(amide imide) phase (as a rigid domain), affecting the flow line of gas permeation [84]. Nagase et al. [86] synthesized siloxane-grafted poly(amide-imide) and PI, which were labeled as PAI-*g*-PDMS and PA-*g*-PDMS with different PDMS segment lengths, respectively (see Fig. 9). The higher aggregation of PI than poly(amide-imide) resulted in the lower solubility of PA-*g*-PDMS than PAI-*g*-PDMS. Accordingly, the permeability coefficients of PAI-*g*-PDMS were higher than those of PA-*g*-PDMS with the same PDMS segment length. The maximum O_2 permeability of PAI-*g*-PDMS was 231 Barrer, whereas the maximum O_2/N_2 selectivity of PA-*g*-PDMS was 2.49 [86].

Park et al. synthesized imide-siloxane/silica hybrid membranes and found a slight decrease in O_2/N_2 selectivity due to the amorphous silica network. In fact, a silica network-matrix interphase was created in the membranes, thereby restricting the chain mobility. The O_2/N_2 selectivity of the hybrid membranes was reported to be 8.7 and 8.0 for 30 and 50 wt% silica contents, respectively [82].

PI-silica composite materials with different tetramethoxysilane (TMOS) molar fractions and silica contents were prepared by Joly et al.,

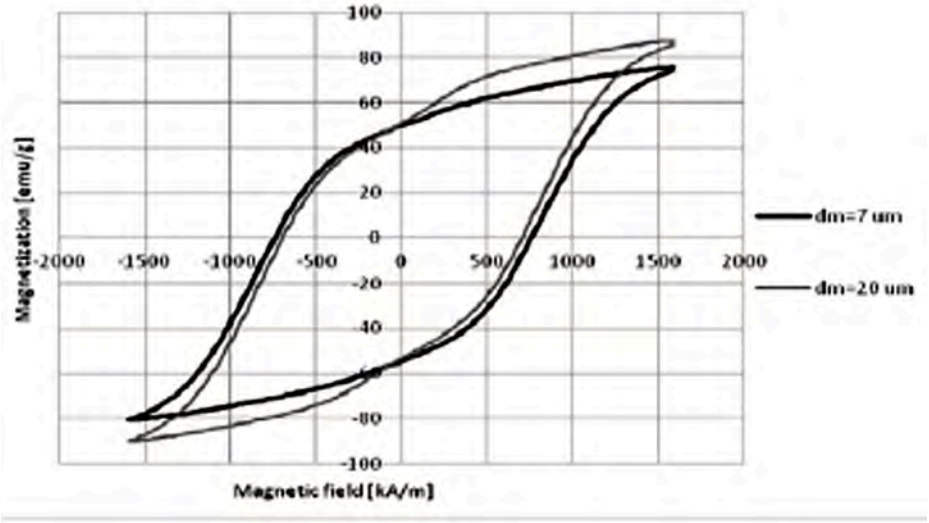

Fig. 15. The comparison between hysteresis loops of membranes containing particles with two different mean diameters (d_m). Reprinted from Ref. [189], Copyright (2017), with permission from Elsevier.

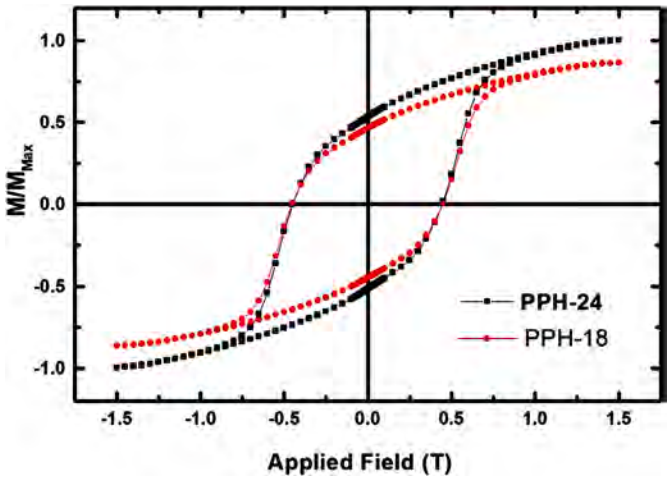

Fig. 16. The comparison between hysteresis loops of MMMs filled with different concentrations (18 and 24 wt%) of $BaFe_{12}O_{19}$ nanoparticles. Reprinted from Ref. [24], Copyright (2020), with permission from Elsevier.

indicating an increase in permeability without the usual loss of the selectivity in the temperature range of 50–150 °C. The O_2 and N_2 permeability of PI-silica composites increased from 0.17 to 0.38 and 0.04 to 0.10 Barrer when increasing the silica content and TMOS molar fraction from 0 to 30 wt% and 25 to 72 wt%, respectively [87]. Lee et al. [88] prepared mixed PDMS/polyether soft segment-based polyurethane ureas (PUU) membranes using a mixture of soft segments with different ratios. The addition of a small amount of polyether (PTMO, PEO, PPO, and PEO-PPO-PEO) into polyether-based PUU membranes decreased permeability without changing the selectivity. In the case of PDMS polyether-based PU membranes, permeability and O_2/N_2 selectivity increased, owing to the creation of the phase separation in both hard (MDI/BD) and soft (polyether) segments, as well as the formation of more tortuous route for diffusing molecules [88]. The investigation of the permeability of polysulphone/polydimethylsiloxane (PSF/PDMS) graft copolymer membranes showed results similar to PDMS membranes and different from PSF ones.

While the permeability of PSF/PDMS copolymer membrane mostly depends on the composition, the corresponding O_2/N_2 selectivity is affected by the PDMS chain length, which is due to the absence of phase separation occurring at the short PDMS branched copolymer. Nagase et al. reported O_2/N_2 selectivity of 2.16 and 2.54 for PSF/PDMS

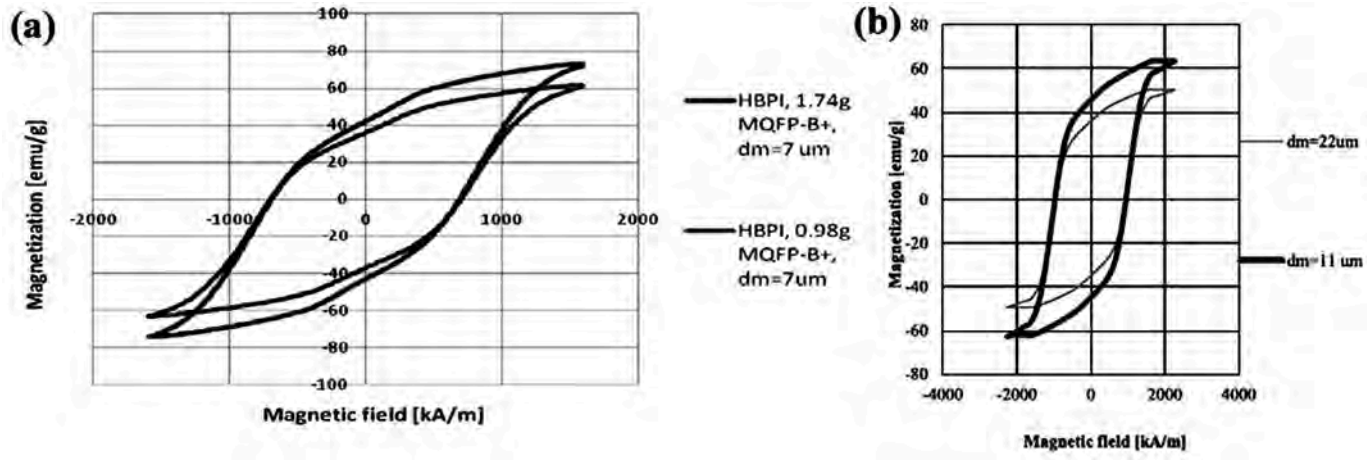

Fig. 17. The comparison between hysteresis loops of membranes with (a) two different filler amounts, reprinted from Ref. [189], Copyright (2017), with permission from Elsevier. and (b) two different d_m. Reprinted from Ref. [183], Copyright (2015), with permission from Elsevier.

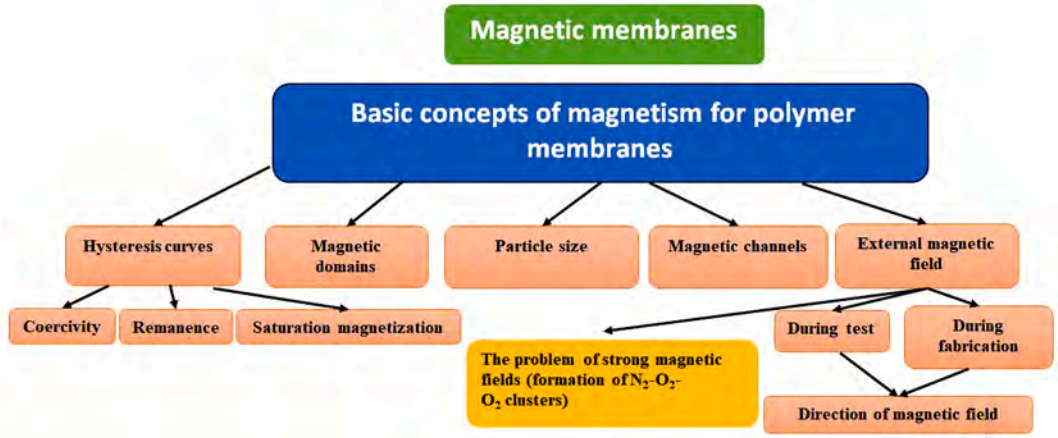

Fig. 18. Basic concepts of magnetism for magnetic polymer membranes.

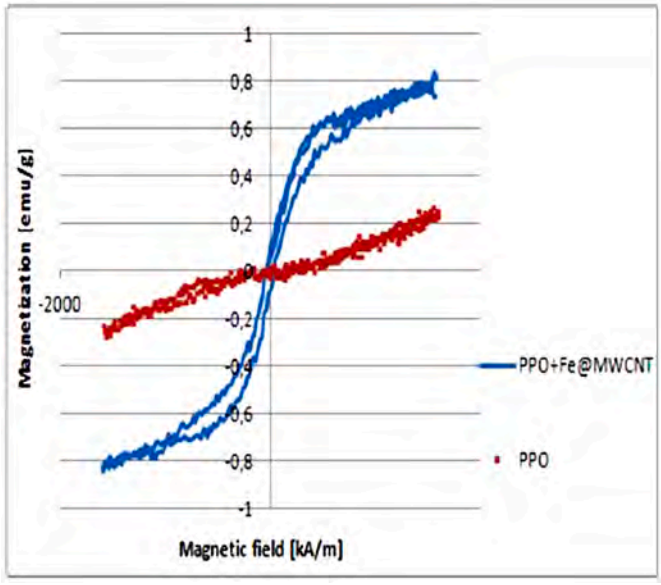

Fig. 19. Hysteresis loops of pure PPO and PPO with Fe@MWCNT, Reprinted from Ref. [177]. Copyright (2018), with permission from Elsevier.

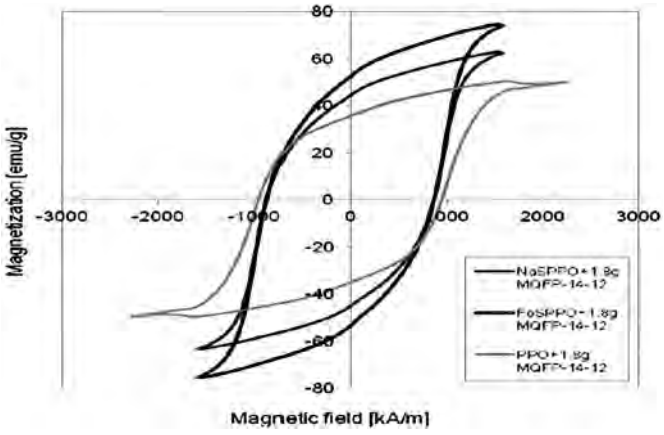

Fig. 20. Hysteresis loops of magnetic hybrid membranes fabricated based on PPO, NaSPPO and FeSPPO polymer matrices with the same filler content. Reprinted from Ref. [193], Copyright (2019),with permission from Elsevier.

membranes with the same composition. In this case, the membrane without the phase separation was under the influence of the polymer backbone component [89].

Kim et al. fabricated hybrid membranes consisting of poly(imide-siloxane) and CNTs. The permeability of O_2 and N_2 was observed to increase as a function of open-ended CNT loading in the matrix of the polymer. For a CNT loading of 10 wt%, the respective permeability of O_2 and N_2 improved from 32.24 to 39.81 Barrer and 11.99 to 17.83 Barrer after the addition of CNTs into PDMS [90]. Roh et al. prepared PDSM membranes with MOF-74 (M = Mg, Mn, Co, and Ni) nanocrystals using microwave reactions, giving rise to rapid and homogenous growth of nanocrystals (NCs). The presence of porous additives, Lewis acidic sites of MOF-74-NCs for O_2, and homogenous dispersion of Mg-MOF-74-NC in the PDMS matrix caused the ideal O_2/N_2 selectivity to be enhanced from 2.1 in PDMS to 4.2 in PDMS/Mn-MOF-74-NC [91].

Xu et al. [92] prepared imide-bridged polysiloxane (PMHS-I) membrane via the reaction of poly(methyhydrosiloxane) with N,N′-bis (3-allyl)pyromellitic diimide, and using Karstedt's catalyst in a one-pot hydrosilylation process (Fig. 10). The creation of small pores (ultra-micropores) and network structure based on imido linkages in the matrix of the membrane enhanced its O_2/N_2 selectivity (4.44) compared to PDMS (2.14). In addition, O_2 permeability (31.0 Barrer) of the membrane was higher than that of pure PI (0.46) [92]. Fig. 11 summarizes modification strategies and overall results of the separation properties of PDMS membranes.

2.6. Poly(arylene sulfone), poly(4-methyl-pentene-1), and polyurethane membranes

Poly(arylene sulfone) (e.g., PSF, and polyethersulfone (PES)), PEBAX, poly(4-methyl-pentene-1) (PMP or TPX), and polyurethane (PU) membranes and their blends with different additives have been used for O_2/N_2 separation properties. The results obtained along with their descriptions are tabulated in the following Tables (1–7).

3. Basic concepts of magnetism in polymeric membranes

The magnetic properties of materials originate from the movement of the electrons of their constituent atoms, thereby creating a magnetic moment [174]. A set of these magnetic moments that are aligned is called a magnetic domain [175]. The domains are the smallest magnetic regions that play an important role in magnetic behavior of particles. The magnetic characteristics of these domains are the final determinant of the magnetization component. Magnetic order of small particles tends to create a single domain, whereas large particles form multiple domains [176].

Ferromagnets, ferrites, and superparamagnets are used in the

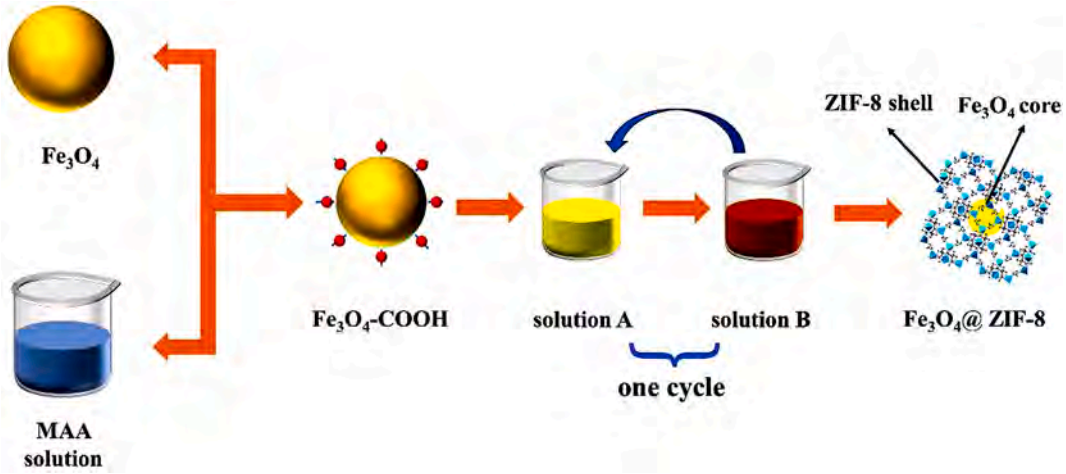

Fig. 21. Schematic representation of the synthesis process of Fe_3O_4@ZIF-8. Reprinted from Ref. [194], Copyright (2024),with permission from Elsevier.

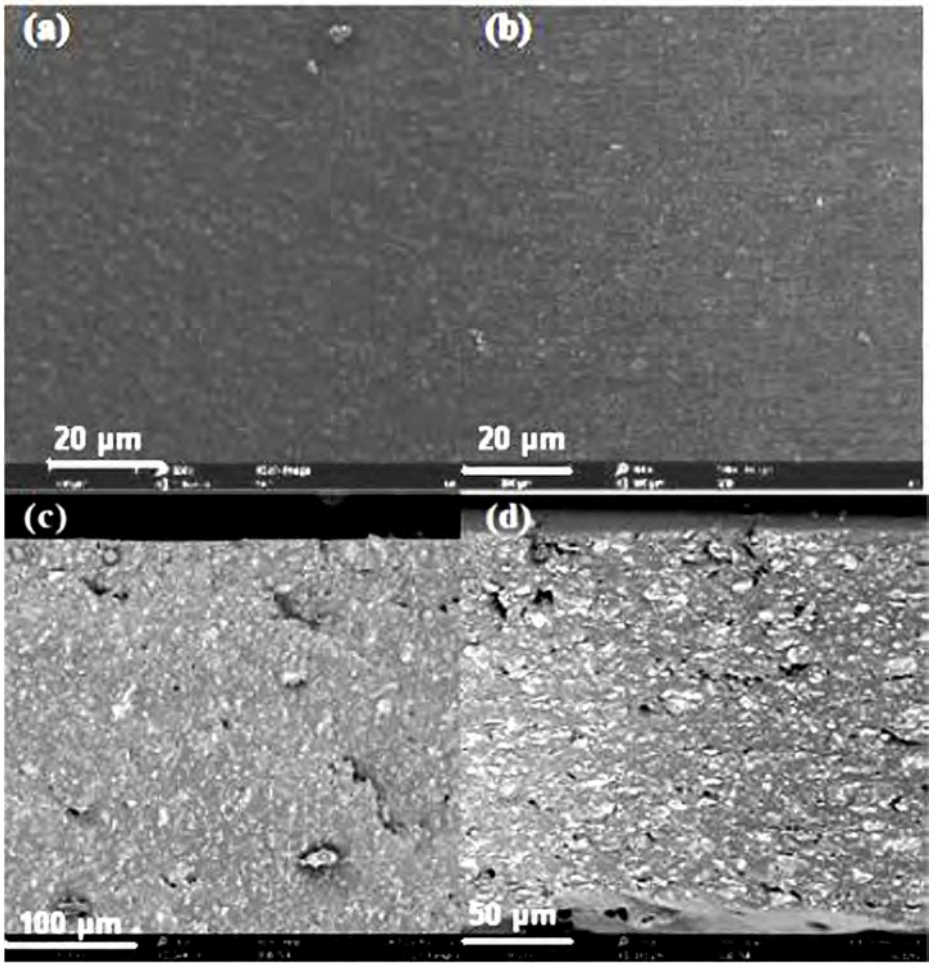

Fig. 22. Top-view SEM images taken to show surface morphology of: (a) parallelly-arranged, and (b) vertically-arranged ATP/PIM-1 MMMs. (c) and (d) The corresponding cross-sectional SEM images. Reprinted from Ref. [202], under a Creative Commons CC-BY-NC-ND license.

fabrication of magnetic flat sheet membranes, possessing magnetic properties due to the formation of magnetic domains. Ferromagnetic materials include cobalt, nickel and iron, and the alloy compounds of these three metals and some rare-earth metals (e.g., Nd) are also known as ferromagnets. Ferrites are a subgroup of ferromagnets, being double oxides of iron and other metals. The permeability of these materials is usually large in the presence of a magnetic field. By applying an external magnetic field to the membrane during its fabrication, the resultant gas separation properties were enhanced [24,177]. For instance, selectivity of PES/Pebax-1657-$BaFe_{12}O_{19}$ magnetic membranes prepared in the absence and presence of magnetic field (perpendicular to the membrane and in the direction of gas transfer) was 2.29 and 2.72, respectively [24].

The magnetic properties of permanent magnets can be evaluated by magnetizing them in the presence of a magnetic field [174]. In the case

Table 8
Magnetic polymer membranes with different additives and magnetic field conditions for O_2/N_2 separation properties.

Polymer	Additive	External Magnetic field or modification	Description	Ref.
EC, PPO	Neodymium (Nd) powder microparticles	Magnetized magnetic membranes under 2.5 T	PPO+ 1.8 g Nd with granulation of 20–32 μm increased O_2 permeability in the magnetic diffusive chamber up to 63 %.	[186]
EC, PPO	MQFP-16(Nd-Fe-B)	Casting in a magnetic field of 32 kA/m	By adding MQFP-16 with granulation of 9 μm into PPO and EC membranes (PPO+1.75 g and EC+1.5 g), O_2/N_2 selectivity in air increased from 3.04 to 1.53 (in the net condition) to 4.36 and 2.94, respectively.	[183]
EC, PPO	MQFP-16(Nd-Fe-B),and MQFP-14-12	Casting in a magnetic field of 40 mT	By adding MQFP-16 and MQFP-14-12 with granulation of 5 and 25 μm into PPO and EC membranes (PPO+1.75 g and EC+1.5 g), O_2/N_2 selectivity in air increased from 3.04 to 1.53 to 4.36 and 2.56, respectively.	[192]
PPO	Fe@MWCNTs	B = 40 and 100 mT	By hydroxylation of Fe@MWCNTs (Fe@MWCNT-OH) and sulfonation of PPO (SPPO) under an external magnetic field, the nanotube-polymer interphase via hydrogen bonding was enhanced, which increased the permeability, diffusivity, and selectivity. For SPPO with 5 wt% of Fe@MWCNT-OH, O_2/N_2 selectivity was found to be 5.15, indicating a significant enhancement in the gas separation compared to the PPO membrane with 5 wt% of Fe@MWCNT (3.45). The hysteresis loops of pure PPO and PPO filled with Fe@MWCNTs showed paramagnetic and ferromagnetic properties (see Fig. 19).	[177]
PPO	Modification by sulfonation and addition of MQPF-12-14		Modification by sulfonation and proton substitution with Na^+ and Fe^{2+} ions caused an improvement in the selectivity from 3.04 to 4 and 4.22 for NaSPPO and FeSPPO, respectively. By adding 1.83 g of MQPF-12-14 fillers, these results showed further improvements, achieving selectivity of 6.88 for NaSPPO and 7.96 for FeSPPO in air. The interaction of the magnetic powder with the iron-containing polymer matrix increased the remanence, saturation magnetization, and the separation factors (see Fig. 20).	[193]
EC, linear polyimide (LPI) or HBPI	MQP-14-12 (Nd powder)	Fabrication at a magnetic field of 40 mT, and using a short magnetic impulse shock of 2.5 T to magnetize the membrane	By adding 1.7 g of MQP-14-12 to HBPI, LPI and EC, the selectivity reached 6.21, 5.07 and 2.55, respectively.	[187]
LPI and HBPI	MQFP-B(Nd-Fe-B) with various granulation (5, 7, 15, and 20 μm)	No external magnetic field	By adding 1.6 g of MQFP-B with $d_m = 7$ and 5 μm to LPI and HBPI, the selectivity increased from 3.25 to 4.10 to 7.24 and 8.69, respectively.	[191]
PPO	MQP-14-12	Fabrication at a magnetic field of 40 mT, and using a short magnetic impulse shock of 2.5 T to magnetize the membrane	O_2/N_2 selectivity increased from 3.4 (PPO) to 4.46 (PPO+1.54g MQP-14) in air separation. Thickness of membrane was 20–181 μm. MQP-14-12 granulation was 5 μm.	[188]
PSF	Carbonyl iron powder (CIP)	The external magnetic field = 570 mT	Addition of 10 wt% of CIP into PSF in the presence of the external magnetic field caused O_2 permeability and selectivity to improve by 436 % and 41 %, respectively.	[180]
PES/Pebax1657 (double-layer membrane)	$BaFe_{12}O_{19}$ (ferrite nanoparticles with high coercivity)	Applying a magnetic field of 0.5 T during the fabrication, and the use of a magnetic module (0.5 T) in the testing process	O_2 and N_2 permeance of the net membrane (without nanoparticles) increased from 0.13490 to 0.07194 in the absence of the external magnetic field to 0.38971 and 0.12754 in the presence of the field, respectively. By adding 24 wt% of $BaFe_{12}O_{19}$ nanoparticles, ideal selectivity improved to 2.72. By adding 24 wt% of $BaFe_{12}O_{19}$ nanoparticles in the presence of the external magnetic field, ideal selectivity further improved to 4.01. The use of the external magnetic field during the test of membranes amplified magnetic domains and magnetic channels.	[24]
PES/Pebax1657 (double-layer membrane)	Fe_3O_4 (superparamagnetic nanoparticles with extremely low coercivity)	Applying different external magnetic fields during the fabrication, along with the use of a magnetic module (0.5 T) in the testing process	While increasing the magnetic field from 0 to 0.3 T did not considerably influence the ideal selectivity, PES/Pebax-Fe_3O_4 membrane exposed to the magnetic field of 0.4 T showed a maximum O_2/N_2 ideal selectivity of 3.59. Thicker channels at the magnetic field of 0.4 T were responsible for higher adsorbing amounts of paramagnetic O_2 molecules using the magnetic module.	[25]
Pebax	Core-shell MOF (Fe_3O_4@ZIF-8)	Preparation and test condition were carried out under a magnetic field	O_2 permeability and O_2/N_2 selectivity of 15 wt% Fe_3O_4@ZIF-8-8/Pebax MMMs reached 194 Barrer and 11.97, respectively. Efficient vertical channels were formed in the membrane by ordering of Fe_3O_4@ZIF during the drying under a magnetic field (see Fig. 21).	[194]

(*continued on next page*)

Table 8 (*continued*)

Polymer	Additive	External Magnetic field or modification	Description	Ref.
PES	Lithium chloride and iron–nickel magnetic alloys ($Fe_{10}Ni_{90}$ starfish-like alloy and $Fe_{20}Ni_{80}$ necklace-like alloy)	No external magnetic field	Permeability increased, whereas the selectivity remained constant due to the poor compatibility of the filler surface and the polymer. PES membranes containing starfish-like $Fe_{10}Ni_{90}$ alloy showed higher efficiency in oxygen transition than PES membranes containing necklace-like $Fi_{20}Ni_{80}$ alloy.	[195]
Cellulose triacetate (CTA)	$Co_{0.5}Ni_{0.5}FeCrO_4$ nanoparticles	Orthogonal magnetic field	By adding $Co_{0.5}Ni_{0.5}FeCrO_4$ magnetic nanoparticles into CTA, gas transport pathways and magnetic trap introduced to the membranes improved the permeability and O_2/N_2 selectivity.	[196]
Cellulose acetate (CA)	Lithium chloride, poly(methylmethacrylate), and iron–nickel magnetic alloys ($Fe_{10}Ni_{90}$ starfish-like alloy and $Fe_{20}Ni_{80}$ necklace-like alloy)	No external magnetic field	Poly(methylmethacrylate) was slightly blended with the membrane in order to improve its mechanical properties. Lithium chloride was used to improve the porosity of the membrane. Membrane containing starfish like $Fe_{10}Ni_{90}$ alloy had a more efficient oxygen transition rate of 1.271×10^{-5} $cm^3/(m^2.s)$ compared to the blank CA membrane.	[197]
Polyvinyl chloride (PVC)	Fe_3O_4/o-MWCNTs	Applying a magnetic field of 0.05 T	Addition of Fe_3O_4/o-MWCNTs nanoparticles and their directional migration to the membrane surface under the magnetic field led to the formation of "moon pit" on the membrane surface.	[198]
PSF	Orthoferrite ($LaFeO_3$)	No external magnetic field	By incorporating 1.0 wt% of $LaFeO_3$ into PSF matrix, the highest O_2/N_2 selectivity (1.42) and higher permeability were obtained compared to the pure PSF membrane.	[199]
Poly(vinylidene fluoride) PVDF	Modification with surface coating (MC) and incorporation of superparamagnetic particles (MM)	Applying a magnetic field of 100 G	Higher O_2 and N_2 permeance from air was observed in PVDF membrane coated with superparamagnetic particles. MC showed the highest value of oxygen permeance from air (3105 GPU).	[200]
PSF	Iron oxide (Fe)	Applying magnetic fields of 330 and 570 mT	O_2 permeability and O_2/N_2 selectivity of PSF-7.5 wt% Fe50 MMMs in the presence of a magnetic field of 570 mT increased about 220 % and 33 %, respectively, being higher than those of neat PSF membranes. By applying the magnetic field during the membrane test, the selectivity of PSF and PSF-Fe membranes was remarkably improved.	[201]
PIM-1	Fe_3O_4 and attapulgite (ATP)	Applying a magnetic field	Fe_3O_4-decorated ATP coated with PDMS was affected by vertical and parallel magnetic fields in the process of evaporation at 25 °C for 2 days, so that the ATP particles were arranged along the direction of the magnetic field line. (see Fig. 22). O_2 permeability coefficient of ~670 Barrer and O_2/N_2 selectivity of ~3 were reported.	[202]

of superparamagnetic nanoparticles, since Brownian rotation time is longer than Néel relaxation time, the magnetization is cancelled out after removing the magnetic field at room temperature. Therefore, the presence of an external magnetic field is necessary during the fabrication of membranes containing superparamagnetic nanoparticles [178]. Strzelewicz et al. obtained a linear relationship between the oxygen air enrichment and the strength of the magnetic field applied to the membrane (see Fig. 13). Due to the small amount of the diffusion coefficient using neodymium powder (20–40 μm), they found that the diffusion process can control the aggregation [179].

The magnetic field applied to the particles helps orient the domains and induce magnetic properties in them. In order to activate magnetic domains, the prepared membrane can be exposed to an external magnetic field or placed in a magnetic module [24], or both of these actions. By using an external magnetic field perpendicular to the surface of membrane, the domains orient towards the field and amplify the magnetic attraction of membrane channels [24]. In this regard, Raveshiyan et al. reported the use of an external magnetic field (570 mT) during the tests of the membrane (MMM containing 7.5 wt% Fe_3O_4 nanoparticles with a size range of 50–100 nm), achieving ~ 220 % and 33 % higher O_2 permeation and selectivity compared to neat PSF membrane [180].

We should distinct between the use of magnetic field during the membrane fabrication and in the separation process. In fact, the use of magnetic field during the membrane fabrication has changed the morphology, crystallinity and chemical state of polymeric membranes, whereas it can help active the magnetic channels when applied during the separation process of magnetic membranes containing particles, keeping in mind that the inducing of the magnetic character to oxygen needs an external magnetic field [24,25]. In other words, the use of an external magnetic field during the membrane fabrication provides the magnetic force required to control the particle dispersion within the polymer matrix. By applying a magnetic field in the direction of membrane thickness, particles in the polymer matrix and distribution of polymer chain packing can be arranged in such as way that pathways between the polymer and particles (so-called magnetic channels) can enhance the separation factors [177].

To understand the magnetic membrane performance, it is necessary to explain the notion of magnetic channels and how paramagnetic oxygen atoms pass through them. The interaction between the channels and paramagnetic molecules was found to take place through molecular spin exchange instead of the long range magnetic field, arising from the smaller contribution of magnetic forces on the molecular motion compared to the strength of thermal fluctuations in the magnetic channels of the polymer membrane [181]. The formation of these magnetic channels occurs near the magnetic granules, creating highway paths for the diffusion of permeating molecules [181]. It can be stated that the Weiss molecular field of the magnet allows for a close approach of paramagnetic O_2 molecules to its surface, which results in their trapping [182]. Compared to the diamagnetic N_2 molecules, paramagnetic O_2 molecules stick to the highway paths on the magnetic

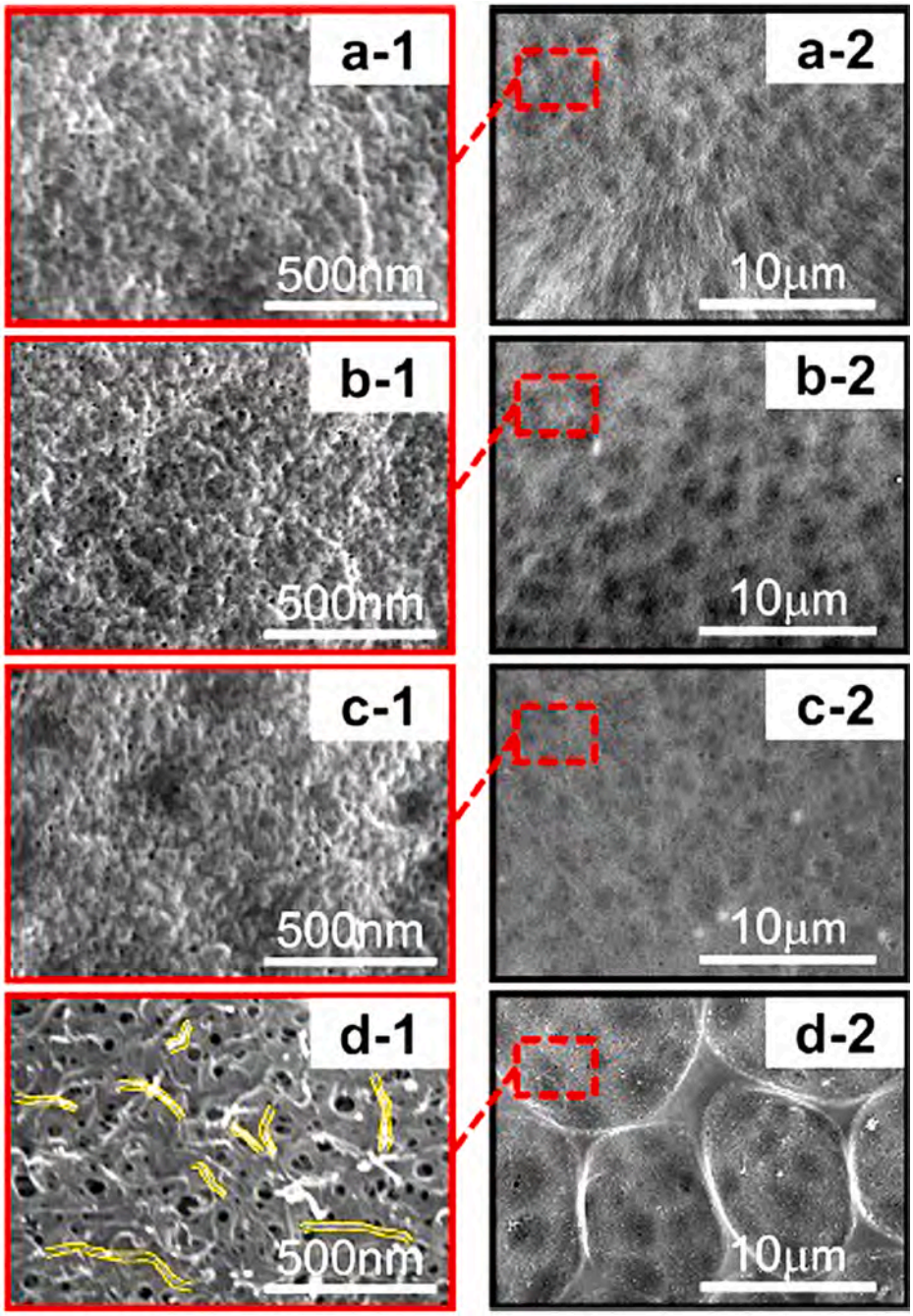

Fig. 23. Surface morphologies of: (a) pristine PVC, (b) MWCNTs/PVC, (c) Fe_3O_4/o-MWCNTs/PVC, and (d) Fe_3O_4/o-MWCNTs/PVC membranes under the effect of a magnetic field. Reprinted from Ref. [198], Copyright (2021),with permission from Elsevier.

channels for a longer time due to their interaction with the Weiss molecular field [181].

Research findings have shown that appropriate composition, small size, and narrow distribution of particles provide the opportunity of fabricating membranes with a homogeneous structure, possessing extensive network of the magnetic channels [180,183]. In this way, the magnetic channels attract paramagnetic oxygen gas molecule and repel diamagnetic nitrogen gas molecule.

Theoretically, the permeation process in polymeric membranes along with the external magnetic field can be described by Smoluchowski equation, indicating a linear relationship between O_2 enrichment and magnetic field strength. For a two-component gas mixture with a potential field, this equation is given by Ref. [179]:

$$\frac{\partial C_1}{\partial t} = D_{11}\frac{\partial^2 C_1}{\partial x^2} + D_{12}\frac{\partial^2 C_2}{\partial x^2} - k\frac{\partial C_1}{\partial x} \quad (1)$$

$$\frac{\partial C_2}{\partial t} = D_{21}\frac{\partial^2 C_1}{\partial x^2} + D_{22}\frac{\partial^2 C_2}{\partial x^2} \quad (2)$$

where C_i (x,t) is the concentration at position x and time t, D_{ij} is the diffusion coefficient, and k is the drift coefficient. The D_{ij} parameter is constant or can depend on distance (D_{ij} (x)), time (D_{ij} (t)), or concentration (D_{ij} (C_i)).

Note that O_2 molecules are paramagnetic, inducing magnetic character to oxygen in the presence of a magnetic field. This arises from the unpaired electrons with spin magnetic moments in the molecule, as well

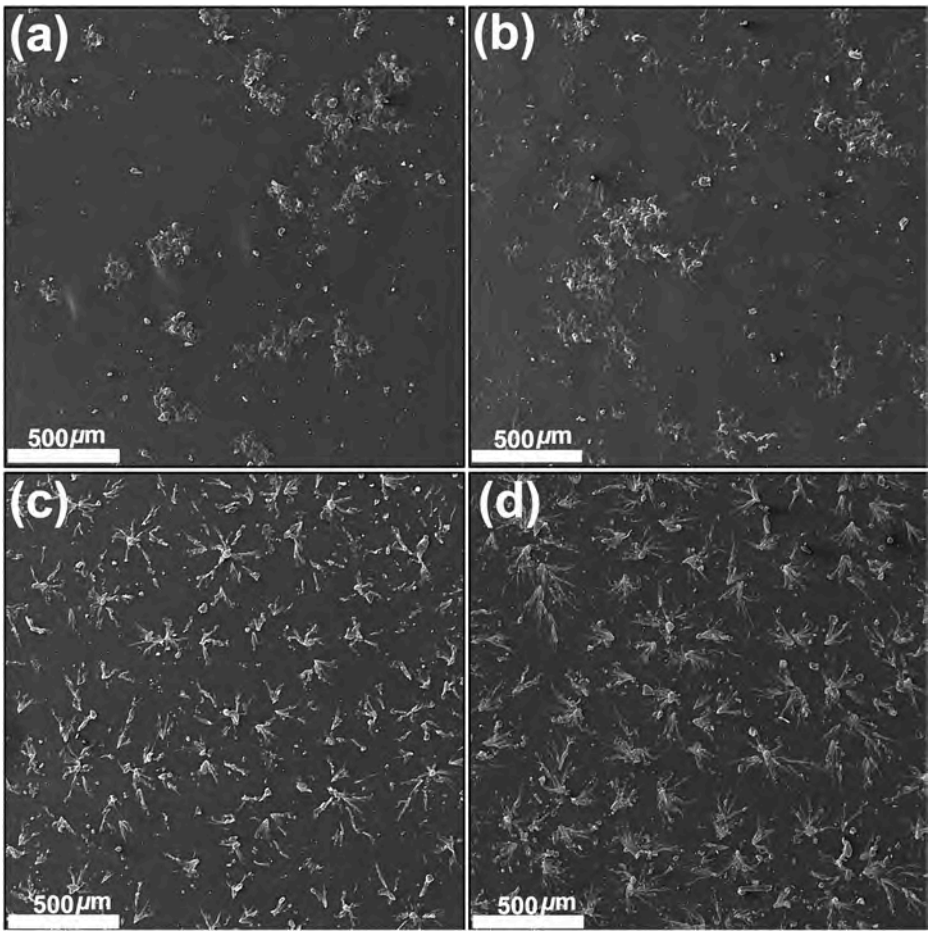

Fig. 24. FE-SEM images of MMMs filled with $BaFe_{12}O_{19}$ nanoparticles: (a) and (b) 18 and 24 wt% $BaFe_{12}O_{19}$ nanoparticles in the absence of a magnetic field, and (c) and (d) 18 and 24 wt% $BaFe_{12}O_{19}$ nanoparticles in the presence of a magnetic field (0.5 T). Reprinted from Ref. [24], Copyright (2020),with permission from Elsevier.

as the negative exchange energy occurring between neighboring oxygen molecules. Therefore, the inducing of the magnetic character to oxygen needs an external magnetic field in the module as a gas container.

In order to theoretically consider polymer-magnetic filler interactions, the fractal analysis through box counting method (BCM) can be used for calculating multifractal parameters, involving a random walk based model to simulate diffusion of magnetic powder particles in polymeric membranes. For a non-interacting particles system, the mean-square displacement of random walk is proportional to a nonlinear function of time as follows [184]:

$$< x^2 > \propto f(t) \tag{3}$$

Because of different granulation and cluster formation in the magnetic membranes, a disordered system should be taken into account, leading to the following relation:

$$< x^2 > \propto t^{\frac{2}{d_w}} \tag{4}$$

where d_w is the dimension of a random walk. For certain type of fractals, this relation turns to:

$$< x^2 > \propto t^{2(2+\theta)} \tag{5}$$

in which: $\theta = 2(d_f - d_s)/d_s$; $d_s = 2\, d_f/d_w$ (6)

The value of fractal dimension (d_f) can be estimated using the BCM. Meanwhile, the estimation of d_w is based on random walk simulation and relation (4). The structures of magnetic powder in membranes have been fractals with $d_f = 1.44$–1.87, possessing stochastic characteristics with smaller complexity, larger homogeneity and self-similarity, which increase with an increase in the amount of magnetic powder and decrease with powder granulation. Thus, d_f increases with an increase in the amount of magnetic powder, and decreases with an increase in the number of condensation nuclei used in simulations.

By increasing powder granulation, d_w decreases, which can be assigned to an increase in the FV of the polymer matrix [185]. For poly (2,6- dimethyl-1,4-phenylene oxide) membranes filled with 1.8 g of praseodymium magnetic powder (granulation of 20–32 mm) in the magnetic diffusive chamber, the structure of the magnetic powder in membranes has been fractals with fractal dimension $d_f = 2.76$–2.84 and stochastic characteristics of $\Delta D = 1.14$–1.32 [186]. Polymer-filler interactions are influenced by forming percolation-like paths and magnetic channels. By adding magnetic powder into the polymer matrix, the distance between magnetic particle chains decreases, leading to an increase in the magnetic interaction between them. This results in the creation of more complex microstructures, being similar to three dimensional (3D) matrices with higher storage modulus.

One of the strategies to optimize the compatibility of polymer-filler interactions is to add magnetic particles into 3D structure of hyperbranched polymers, thereby creating a more developed network of permeation pathways, while also increasing the magnetic membrane selectivity. In this regard, hyperbranched polyimide (HBPI) [187] and PPO [188]can disaggregate N_2–O_2–O_2 and create O_2–O_2–O_2 clusters, resulting in an increase in the separation performance. Also, by employing a co-casting method, water as a solvent of the top layer of membrane with hydrophilic substrate in the presence of an external

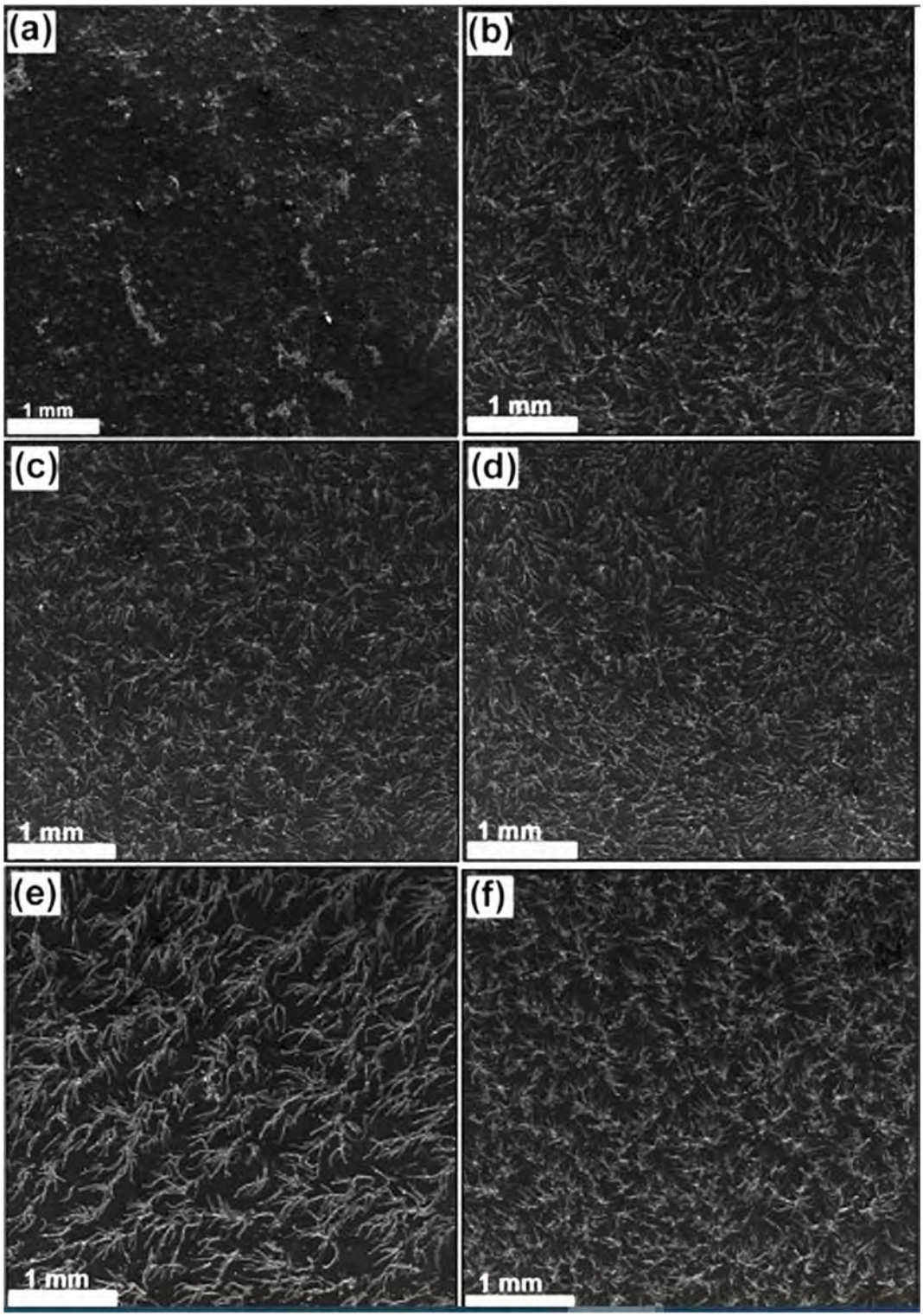

Fig. 25. FE-SEM images of PES/Pebax-Fe_3O_4 membranes exposed to an external magnetic field with intensity of: (a) 0 T, (b) 0.1 T, (c) 0.2 T, (d) 0.3 T, (e) 0.4 T, and (f) 0.5 T. Reprinted from Ref. [24],Copyright (2021),with permission from Elsevier.

magnetic field can improve the compatibility [24,25]. It should be noted that some polymers such as PPO have shown hysteresis loops, indicating their weak magnetic behavior with enhanced air separation properties [177].

3.1. Magnetic characteristics of magnetic membranes

The most conventional approach to characterizing magnetic membranes is the hysteresis loop measurements, providing important information about magnetic parameters of the filler used in the membranes. These parameters include coercivity, remanence and saturation magnetization, which are described in the following sections.

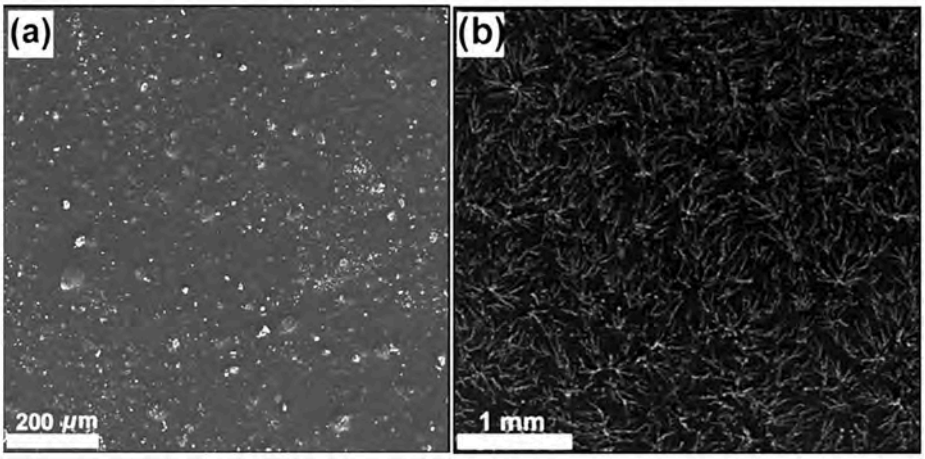

Fig. 26. (a) and (b) FE-SEM images of Pebax-Fe_3O_4 and PES/Pebax-Fe_3O_4 membranes exposed to an external magnetic field, respectively. Reprinted from Ref. [25], Copyright (2021),with permission from Elsevier.

3.1.1. Coercivity

As a magnetic parameter, coercivity is defined as the magnetic field required to decrease the magnetization to zero after the magnetic material has reached its saturation state. Among the magnetic materials, ferromagnetic and ferrite particles (categorized as soft materials) have significantly lower coercivity than hard (permanent) magnetic materials. Meanwhile, the coercivity of superparamagnetic particles is almost zero. The value of coercivity increases with decreasing the magnetic filler granulation and particle size distribution in polymeric membranes [189,190], involving the surface anisotropy and interparticle interactions. On the other hand, the coating of magnetic powders with polymer influences the net magnetic anisotropy. In other words, a reduction in the effective magnetocrystalline anisotropy by the polymer coating will lead to a decrease in coercivity [183,189]. For instance, the coercivity of PI combined with Nd-Fe-B particles with a mean diameter (d_m) of 20 μm was considerably lower than that of PI combined with d_m = 5 μm [189], as shown in Figs. 14 and 15. Of course, it should be noted that the reduction of coercivity depends on the polymer coating's characteristics. Rybak et al. indicated that the coercivity has an indirect influence on gas separation factors, involving the magnetic remanence and the decrease in particle size [183]. It is worth noting that the concentration of the filler may not change the hysteresis loop coercivity, as found for MMMs filled with 18 and 24 wt% $BaFe_{12}O_4$ nanoparticles (Fig. 16). The addition of Fe@MWCNTs into poly(2,6-dimethyl-1, 4-phenylene oxide) (PPO) at a weaker magnetic field (40 mT) decreased the coercivity, which was assigned to the formation of agglomerates. At a stronger magnetic field (100 mT), the coercivity remained almost constant, which was related to the more homogeneous distribution of Fe@MWCNTs in the polymer matrix [177].

3.1.2. Magnetic remanence and saturation

The magnetic remanence is defined as the magnetization that remains in the material after the removal of the external magnetic field. The changes in size or number of magnetic domains induced by the magnetic field can influence the remanence. Also, it is affected by the magnetic powder content and microstructure of particles [189]. It has been shown that the remanence increases by adding the amount of magnetic powder in the membrane, leading to an exponential increase in the gas separation coefficient factors [183]. By adding approximately 1.7 g of NdFeB microparticles with d_m = 7 μm into the linear (ODPA-MDA) and hyperbranched (ODPA-MTA) polymers, remanence and saturation magnetization were observed to increase, giving rise to an improvement in the gas transport and selectivity coefficients of the membranes [189]. Also, Rybak reported an increase in the remanence and saturation magnetization when using different amounts of the filler, according to Fig. 17(a). In this case, increasing the particle size from d_m = 11–22 μm decreased the corresponding remanence and saturation magnetization (see Fig. 17(b)) [183]. Note that the saturation magnetization was linearly dependent on the magnetic filler additive, and that the influence of remanence on the separation factors and transport properties was significantly greater than saturation magnetization [183].

It has been documented that the saturation magnetization of bulk magnetic powder particles is considerably larger than that of the magnetic membrane, resulting from the chemical environment (polymers and surfactants) influence on the magnetization of particles and membrane. For example, saturation magnetization of bulk powder was 105.66 emu/g, whereas that of the magnetic membrane was 63.86 emu/g [183]. In fact, real systems have variable factors such as polydispersity, shape anisotropy, surface morphology and bonding chemistry, affecting the magnetic properties [183].

The presence of particles in the polymer chain packing creates channels in the matrix. By using an external magnetic field in direction of membrane thickness during the membrane casting, these channels with ferromagnetic, ferrimagnetic and superparamagnetic domains are arranged and activated along the external magnetic field direction, improving oxygen absorption when using the external magnetic field during gas separation. As mentioned earlier, the coercivity has an indirect influence on gas separation factors, involving magnetic remanence and particle size. Superparamagnetic particles associate with a decrease in powder particle size. The constituent particles are so small that they form a single domain and have no walls, resulting in an almost zero coercivity. The microstructural studies of magnetic membranes have confirmed the fabrication of membranes with homogeneous structure using powders with appropriate composition and smaller particle size and distribution due to their larger surface area and adhesive capacity [190,191].

By decreasing particle size of the magnetic powder, remanence and coercivity increase, improving gas separation factors. On the other hand, decreasing the granule size reduces the aggregation that provides a larger surface available for the magnetic channels. In other words, larger surface decreases the probability of meeting O_2 and N_2 molecules, which leads to a smaller aggregation rate. In the case of higher concentration of magnetic particles in a polymer solution, the phenomenon of sedimentation has been observed, in conjunction with further aggregation and heterogeneous distribution of particles in the polymer matrix, thereby deteriorating the gas separation factors [181]. In summary, Fig. 18 shows basic concepts of magnetism when considering magnetic polymer membranes. Also, the magnetic polymer membranes along with their additives used for O_2/N_2 separation properties are tabulated in Table 8.

3.2. Orientation of magnetic particles in polymeric membranes

The presence of magnetic fields during the membrane fabrication may assist the mixing of magnetic nanoparticle in the matrix of polymers. Earlier, we indicated how the magnetic field helped avoid agglomeration, while also orienting the nanoparticles in the magnetic field direction. Liu et al. demonstrated the magnetic field effect on surface morphologies of PVC, MWCNTs/PVC, Fe_3O_4/o-MWCNTs/PVC and Fe_3O_4/o-MWCNTs/PVC membranes [198], as shown in Fig. 23. Also, they found significantly higher Fe content in the upper edge of the membrane compared to the lower edge, which was ascribed to the magnetic field effect [198]. Other researcher groups reported the formation of efficient vertical channels in the membrane by arrangement of nanomagnetic particles (Fe_3O_4@ZIF) during the membrane drying under a magnetic field [194].

Alternatively, the effect of magnetic field on the morphology of MMMs filled with $BaFe_{12}O_{19}$ nanoparticles (18 and 24 wt%) has been investigated (see Fig. 24). As observed, the random accumulation of $BaFe_{12}O_{19}$ nanoparticles on the Pebax polymer surface turned into the bundles of flower-like nanoparticles after the magnetic field exposure, which could improve the functionality of the surface.

3.3. The interplay between magnetic field intensity and nanoparticle orientation

The magnetic field intensity can change the surface morphology of polymeric membranes when it comes to the use of magnetic nanoparticles as fillers. Notably, PES/Pebax-Fe_3O_4 membranes, fabricated using a co-casting method, were exposed to different intensities of an external magnetic field (0–0.5 T) during their fabrication. FE-SEM images of these membranes are shown in Fig. 25. A higher value of ideal O_2/N_2 selectivity was obtained at the magnetic field intensity of 0.4 T, which was assigned to stronger interactions between Fe_3O_4 nanoparticles with superparamagnetic behavior to form thicker channels. A remarkable experiment was the effect of the magnetic field on the Pebax polymer solvent i.e. water. Due to their diamagnetic nature, water molecules (acting as the polymer solvent) were repelled by the magnetic field, and the PES (as the hydrophilic polymer solved in DMF) attracted them, thus decreasing the crystalline region and increasing the chain mobility of the polymer, which improved the permeance of the membranes. This effect of the magnetic field on the water solvent was not observed in the single-layer membrane (without PES), according to Fig. 26 [25].

3.4. The formation of N_2–O_2–O_2 clusters in the presence of magnetic fields

Tagiro et al. reported the formation of O_2–O_2–O_2, N_2–O_2–O_2, and N_2–N_2–O_2 cluster types in the presence of sufficiently strong magnetic fields. By calculating the bonding energy and electron paramagnetic resonance, they found that the first two types were more desirable [203]. When the magnetic field was applied to the membranes, the diamagnetic nitrogen clusters (N_2–O_2–O_2) dragged into the magnetic channels, transported N_2, and created aggregations due to the development of large magnetic dipoles on the clusters and their interaction with the magnetic field, leading to a less effective process in separation of O_2 from air [182,186,188,204,205]. In this way, Rybak et al. used polymer matrices such as LPI, HBPI and PPO along with magnetic powders in order to prevent the aggregation of N_2–O_2–O_2 clusters, while also improving oxygen enrichment by creating O_2–O_2–O_2 clusters [188,204]. They found that the use of a more uniform magnetic field for the PI magnetic membrane can lower the possibility of the formation of N_2–O_2–O_2 clusters. A significant increase in the gas diffusivity of heterogeneous membranes was observed compared to homogeneous ones [187]. The aggregation of O_2 and N_2 to form O_2–N_2 can be broken by discontinuities at disordered domain walls of the magnetic granule. Decreasing the granule size results in a larger surface of the magnetic channels, thus lowering the probability of the formation of O_2–N_2 [181]. In fact, the formation of molecular clusters can lead to differences between theoretical and experimental results [206].

4. Conclusions

We have reviewed the formation, structure, and O_2/N_2 separation properties of a wide variety of polymeric membranes and MMMs, including PI, PTMSP, PIM, PDMS, ZIF-8, PES, PEBAX, PMP, TPX, PU, etc. Many additives (e.g., nanoparticles, SWNTs, MWCNTs, silica, BM, zeolites, Al_2O_3, TiO_2, ZnO, etc.) and treatments (e.g., crosslinking, chlorination, fluorine exposure, aging, plasma treatment, copolymerization, UV photografting, etc.) were introduced in order to enhance permeability and selectivity of the membranes. Some parameters such as particle size and dispersion, solvent type and concentration, temperature, pressure, sheet thickness, synthesis method, and polymer textures were found to play roles in the separation results. In this regard, TPX, PIM, and some organic/inorganic additives such as TiO_2, BM, and zeolites were promising.

On the other hand, basic concepts of magnetism in the membranes along with magnetic polymer membranes with different additives and magnetic field conditions were discussed for O_2/N_2 separation properties, proposing promising perspectives for O_2/N_2 separation due to the different magnetic properties of oxygen (paramagnetic) and nitrogen (diamagnetic) gases. By increasing the concentration of particles, the gas transport and selectivity coefficients of the membranes were enhanced due to the increase in both remanence and saturation magnetization. The former was linearly dependent on the magnetic filler additive, whereas the influence of remanence on the separation factors and transport properties was significantly greater. The coercivity had an indirect influence on gas separation factors, involving the magnetic remanence and the decrease in particle size. The majority of MMMs suffered from particles accumulation and activation of magnetic domains and nano-channels, which could be solved by using external magnetic fields during the fabrication and separation process. However, the formation of N_2–O_2–O_2 clusters and particles driven to the membrane edge under a strong magnetic field during the fabrication limited the separation results. Undoubtedly, significant research and development are still needed to enhance separation properties of polymeric membranes and MMMs.

Industrial applications of the polymeric and MMM flat sheets can be realized by incorporating organic and inorganic fillers in the membrane matrix. However, large-scale oxygen enrichment based on magnetic membranes is challenging, requiring the synthesis of new materials and membrane fabrication methods. Computational simulations of magnetic particles, polymer structure and polymer-filler interactions by molecular dynamics, density functional theory, and LAMMPS computations should be accompanied with experimental results in order to create a hybrid model with optimized membrane performance for efficient separation purposes.

CRediT authorship contribution statement

Nahid Nikpour: Writing – original draft, Visualization, Conceptualization. **Amir H. Montazer:** Writing – review & editing, Validation.

Declaration of competing interest

The authors declare that they have no known competing financial interests or personal relationships that could have appeared to influence the work reported in this paper.

Data availability

This manuscript is a Review Paper.

References

[1] T. Araújo, T. da Silva Lopes, G. Bernardo, A. Mendes, Techno-economic analysis of carbon molecular sieve membranes to produce oxygen enrichment air, J. Membr. Sci. 694 (2024) 122430.

[2] M.A. Farea, H.Y. Mohammed, S.M. Shirsat, M.-L. Tsai, M.N. Murshed, M.E. El Sayed, S. Naji, A. Samir, R.M. Alsharabi, M.D. Shirsat, A novel approach for ultrafast and highly sensitive carbon monoxide gas sensor based on PEDOT/GO nanocomposite, Mater. Sci. Semicond. Process. 155 (2023) 107255.

[3] H. Ragab, N. Diab, G.M. Aleid, R. Ab Aziz, N. Yusof, M.A. Farea, High-performance NO2 sensing with SnO2/rGO/PEDOT composite for advanced pollution control applications, Inorg. Chem. Commun. (2025) 114133.

[4] M.A. Farea, H.Y. Mohammed, S.M. Shirsat, Z.M. Ali, M.-L. Tsai, I. Yahia, H. Zahran, M.D. Shirsat, Impact of reduced graphene oxide on the sensing performance of poly (3, 4–ethylenedioxythiophene) towards highly sensitive and selective CO sensor: a comprehensive study, Synth. Met. 291 (2022) 117166.

[5] M.A. Farea, N. Yusof, H.Y. Mohammed, M.N. Murshed, A. Samir, A. Hendi, A. Osman, Enhanced NO2 sensing performance of CdS nanoparticle-modified PEDOT: PSS composite: a systematic study of ultrasensitivity and reliability, Colloids Surf. A Physicochem. Eng. Asp. 703 (2024) 135305.

[6] D.A. Fitzgerald, R.J.H. Massie, G.M. Nixon, A. Jaffe, A. Wilson, L.I. Landau, J. Twiss, G. Smith, C. Wainwright, M. Harris, Infants with chronic neonatal lung disease: recommendations for the use of home oxygen therapy, Med. J. Aust. 189 (2008) 578–582.

[7] J. Pasek, S. Szajkowski, V. Travagli, G. Cieślar, Topical hyperbaric oxygen therapy versus local ozone therapy in healing of venous leg ulcers, Int. J. Environ. Res. Publ. Health 20 (2023) 1967.

[8] C. Kamiya, K. Odagiri, N. Inui, T. Suda, H. Watanabe, Pulmonary hypertension associated with diffuse panbronchiolitis that improved with erythromycin and home oxygen therapy, Intern. Med. 62 (2023) 2231–2236.

[9] C. Yang, Q. Yang, Y. Xiang, X.-R. Zeng, J. Xiao, W.-D. Le, The neuroprotective effects of oxygen therapy in Alzheimer's disease: a narrative review, Neural Regenera. Res. 18 (2023) 57–63.

[10] B. Adhikari, C.J. Orme, J.R. Klaehn, F.F. Stewart, Technoeconomic analysis of oxygen-nitrogen separation for oxygen enrichment using membranes, Separ. Purif. Technol. 268 (2021) 118703.

[11] B. Belaissaoui, Y. Le Moullec, H. Hagi, E. Favre, Energy efficiency of oxygen enriched air production technologies: Cryogeny vs membranes, Separ. Purif. Technol. 125 (2014) 142–150.

[12] A.F. Ismail, K. Chandra Khulbe, T. Matsuura, A.F. Ismail, K.C. Khulbe, T. Matsuura, Membrane fabrication/manufacturing Techniques, Gas Separation Membranes: Polymeric and Inorganic, 2015, pp. 193–220.

[13] Y. Li, G. He, S. Wang, S. Yu, F. Pan, H. Wu, Z. Jiang, Recent advances in the fabrication of advanced composite membranes, J. Mater. Chem. A 1 (2013) 10058–10077.

[14] Y. Yampolskii, B. Freeman, Membrane Gas Separation, 2010.

[15] S. Arizzi, P. Mott, U. Suter, Space available to small diffusants in polymeric glasses: analysis of unoccupied space and its connectivity, J. Polym. Sci. B Polym. Phys. 30 (1992) 415–426.

[16] D. Bastani, N. Esmaeili, M. Asadollahi, Polymeric mixed matrix membranes containing zeolites as a filler for gas separation applications: a review, J. Ind. Eng. Chem. 19 (2013) 375–393.

[17] P. Bernardo, E. Drioli, G. Golemme, Membrane gas separation: a review/state of the art, Ind. Eng. Chem. Res. 48 (2009) 4638–4663.

[18] Y. Yampolskii, A. Alentiev, G. Bondarenko, Y. Kostina, M. Heuchel, Intermolecular interactions: new way to govern transport properties of membrane materials, Ind. Eng. Chem. Res. 49 (2010) 12031–12037.

[19] P. Ignatusha, H. Lin, N. Kapuscinsky, L. Scoles, W. Ma, B. Patarachao, N. Du, Membrane separation technology in direct air capture, Membranes 14 (2024) 30.

[20] R. Singh, B. Prasad, Y.-H. Ahn, Recent developments in gas separation membranes enhancing the performance of oxygen and nitrogen separation: a comprehensive review, Gas Sci. Eng. (2024) 205256.

[21] L.T.d.M. de Sousa, S.A. Altino, Construction and analysis of a detailed new database for gas separation membranes, Obs. De La Econ. Latinoam 22 (2024) e3839–e3840.

[22] T.T. Moore, W.J. Koros, Non-ideal effects in organic–inorganic materials for gas separation membranes, J. Mol. Struct. 739 (2005) 87–98.

[23] R.D. Noble, Perspectives on mixed matrix membranes, J. Membr. Sci. 378 (2011) 393–397.

[24] N. Nikpour, B. Khoshnevisan, Enhanced selectivity of O2/N2 gases in co-casted mixed matrix membranes filled with BaFe12O19 nanoparticles, Separ. Purif. Technol. 242 (2020) 116815.

[25] N. Nikpour, A.H. Montazer, A. Khayatian, Magnetic field-induced improvement in O2/N2 gas separation applications of simultaneously co-casted superparamagnetic mixed matrix membranes, J. Ind. Eng. Chem. 105 (2022) 530–538.

[26] C.-C. Hu, P.-H. Cheng, S.-C. Chou, C.-L. Lai, S.-H. Huang, H.-A. Tsai, W.-S. Hung, K.-R. Lee, Separation behavior of amorphous amino-modified silica nanoparticle/polyimide mixed matrix membranes for gas separation, J. Membr. Sci. 595 (2020) 117542.

[27] Y. Feng, J. Ren, H. Li, D. Zhao, L. Sheng, Y. Wu, W. Zhao, M. Deng, Effect of thermal annealing on gas separation performance and aggregation structures of block polyimide membranes, Polymer 219 (2021) 123538.

[28] L. Escorial, M. de la Viuda, S. Rodríguez, A. Tena, A. Marcos, L. Palacio, P. Prádanos, A.E. Lozano, A. Hernández, Partially pyrolized gas-separation membranes made from blends of copolyetherimides and polyimides, Eur. Polym. J. 103 (2018) 390–399.

[29] S. Wu, J. Liang, Y. Shi, M. Huang, X. Bi, Z. Wang, J. Jin, Design of interchain hydrogen bond in polyimide membrane for improved gas selectivity and membrane stability, J. Membr. Sci. 618 (2021) 118659.

[30] C. Álvarez, Á.E. Lozano, M. Juan-y-Seva, J.G. de la Campa, Gas separation properties of aromatic polyimides with bulky groups. Comparison of experimental and simulated results, J. Membr. Sci. 602 (2020) 117959.

[31] C.-Y. Park, E.-H. Kim, J.H. Kim, Y.M. Lee, J.-H. Kim, Novel semi-alicyclic polyimide membranes: synthesis, characterization, and gas separation properties, Polymer 151 (2018) 325–333.

[32] C. Wang, Z. Cai, W. Xie, Y. Jiao, L. Liu, L. Gong, Q.-W. Zhang, X. Ma, H. Zhang, S. Luo, Finely tuning the microporosity in dual thermally crosslinked polyimide membranes for plasticization resistance gas separations, J. Membr. Sci. 659 (2022) 120769.

[33] H. Sun, C. Ma, B. Yuan, T. Wang, Y. Xu, Q. Xue, P. Li, Y. Kong, Cardo polyimides/TiO2 mixed matrix membranes: synthesis, characterization, and gas separation property improvement, Separ. Purif. Technol. 122 (2014) 367–375.

[34] C. Zhang, Synthesis and characterization of bis (Phenyl) fluorene-based cardo polyimide membranes for H2/CH4 separation, J. Mater. Sci. 54 (2019) 10560–10569.

[35] C. Zhang, B. Cao, P. Li, Thermal oxidative crosslinking of phenolphthalein-based cardo polyimides with enhanced gas permeability and selectivity, J. Membr. Sci. 546 (2018) 90–99.

[36] Y. Lu, J. Hao, L. Li, J. Song, G. Xiao, H. Zhao, Z. Hu, T. Wang, Preparation and gas transport properties of thermally induced rigid membranes of copolyimide containing cardo moieties, React. Funct. Polym. 119 (2017) 134–144.

[37] S. Zhang, X. Lu, M. Cai, Z. Wang, Z. Han, Z. Chen, R. Liu, K. Li, Y. Min, Attapulgite nanorod-incorporated polyimide membrane for enhanced gas separation performance, Polymers 14 (2022) 5391.

[38] F. Wang, B. Zhang, S. Liu, Y. Wu, T. Wang, J. Qiu, Investigation of the attapulgite hybrid carbon molecular sieving membranes for permanent gas separation, Chem. Eng. Res. Des. 151 (2019) 146–156.

[39] T. Masuda, E. Isobe, T. Higashimura, K. Takada, Poly [1-(trimethylsilyl)-1-propyne]: a new high polymer synthesized with transition-metal catalysts and characterized by extremely high gas permeability, J. Am. Chem. Soc. 105 (1983) 7473–7474.

[40] K. Takada, H. Matsuya, T. Masuda, T. Higashimura, Gas permeability of polyacetylenes carrying substituents, J. Appl. Polym. Sci. 30 (1985) 1605–1616.

[41] Y. Ichiraku, S. Stern, T. Nakagawa, An investigation of the high gas permeability of poly (1-trimethylsilyl-1-propyne), J. Membr. Sci. 34 (1987) 5–18.

[42] T. Masuda, E. Isobe, T. Higashimura, Polymerization of 1-(trimethylsilyl)-1-propyne by halides of niobium (V) and tantalum (V) and polymer properties, Macromolecules 18 (1985) 841–845.

[43] T. Masuda, Y. Iguchi, B.-Z. Tang, T. Higashimura, Diffusion and solution of gases in substituted polyacetylene membranes, Polymer 29 (1988) 2041–2049.

[44] R. Srinivasan, S. Auvil, P. Burban, Elucidating the mechanism (s) of gas transport in poly [1-(trimethylsilyl)-1-propyne](PTMSP) membranes, J. Membr. Sci. 86 (1994) 67–86.

[45] L. Shao, J. Samseth, M.B. Hägg, Crosslinking and stabilization of nanoparticle filled poly (1-Trimethylsilyl-1-Propyne) nanocomposite membranes for gas separations, J. Appl. Polym. Sci. 113 (2009) 3078–3088.

[46] T. Nakagawa, T. Saito, S. Asakawa, Y. Saito, Polyacetylene derivatives as membranes for gas separation, Gas Separ. Purif. 2 (1988) 3–8.

[47] T.C. Merkel, Z. He, I. Pinnau, B.D. Freeman, P. Meakin, A.J. Hill, Effect of nanoparticles on gas sorption and transport in poly (1-trimethylsilyl-1-propyne), Macromolecules 36 (2003) 6844–6855.

[48] G. Golubev, I. Borisov, E. Litvinova, V. Khotimsky, D. Bakhtin, A. Pastukhov, V. Davankov, V. Volkov, A novel hybrid material based on polytrimethylsilylpropyne and hypercrosslinked polystyrene for membrane gas separation and thermopervaporation, Petrol. Chem. 57 (2017) 498–510.

[49] D. Gomes, S.P. Nunes, K.-V. Peinemann, Membranes for gas separation based on poly (1-trimethylsilyl-1-propyne)–silica nanocomposites, J. Membr. Sci. 246 (2005) 13–25.

[50] S. Matson, I. Levin, A. Ezhov, V. Makrushin, E. Litvinova, V. Khotimskiy, The supramolecular organization and surface morphology of films of poly (1-trimethylsilyl-1-propyne) with different configurational compositions, Membranes Membrane Technol. 2 (2020) 310–317.

[51] V. Makrushin, A. Kossov, V. Polevaya, I. Levin, D. Bezgin, D. Syrtsova, S. Matson, The effect of stereoregularity and adding irganox 1076 on the physical aging behavior of poly (1-trimetylsilyl-1-propyne), Polymers 15 (2023) 2172.

[52] S. Shishatskiy, V. Makrushin, I. Levin, P. Merten, S. Matson, V. Khotimskiy, Effect of immobilization of phenolic antioxidant on thermo-oxidative stability and aging of poly (1-trimethylsilyl-1-propyne) in view of membrane application, Polymers 14 (2022) 462.

[53] G. Golubev, D. Bakhtin, S. Makaev, I. Borisov, A. Volkov, Hybrid microporous polymeric materials with outstanding permeability and increased gas transport stability: PTMSP aging prevention by sorption of the polymerization catalyst on HCPS, Polymers 13 (2021) 1922.

[54] A. Kossov, V. Makrushin, I. Levin, S. Matson, The effect of thermal annealing on the structure and gas transport properties of poly (1-trimethylsilyl-1-propyne) films with the addition of phenolic antioxidants, Polymers 15 (2023) 286.

[55] M. Carta, R. Malpass-Evans, M. Croad, Y. Rogan, J.C. Jansen, P. Bernardo, F. Bazzarelli, N.B. McKeown, An efficient polymer molecular sieve for membrane gas separations, Science 339 (2013) 303–307.

[56] X. Chen, L. Wu, H. Yang, Y. Qin, X. Ma, N. Li, Tailoring the microporosity of polymers of intrinsic microporosity for advanced gas separation by atomic layer deposition, Angew. Chem. Int. Ed. 60 (2021) 17875–17880.
[57] X. Ma, H.W. Lai, Y. Wang, A. Alhazmi, Y. Xia, I. Pinnau, Facile synthesis and study of microporous catalytic arene-norbornene annulation–troger's base ladder polymers for membrane air separation, ACS Macro Lett. 9 (2020) 680–685.
[58] M. Carta, M. Croad, R. Malpass-Evans, J.C. Jansen, P. Bernardo, G. Clarizia, K. Friess, M. Lanč, N.B. McKeown, Triptycene induced enhancement of membrane gas selectivity for microporous Tröger's base polymers, Adv. Mater. 26 (2014) 3526.
[59] R. Williams, L.A. Burt, E. Esposito, J.C. Jansen, E. Tocci, C. Rizzuto, M. Lanč, M. Carta, N.B. McKeown, A highly rigid and gas selective methanopentacene-based polymer of intrinsic microporosity derived from Tröger's base polymerization, J. Mater. Chem. A 6 (2018) 5661–5667.
[60] E. Aliyev, J. Warfsmann, B. Tokay, S. Shishatskiy, Y.-J. Lee, J. Lillepaerg, N. R. Champness, V. Filiz, Gas transport properties of the metal–organic framework (MOF)-Assisted polymer of intrinsic microporosity (PIM-1) thin-film composite membranes, ACS Sustain. Chem. Eng. 9 (2020) 684–694.
[61] B.D. Freeman, Basis of permeability/selectivity tradeoff relations in polymeric gas separation membranes, Macromolecules 32 (1999) 375–380.
[62] N. Li, X. Chen, Y. Fan, L. Zhang, D. Guan, C. Ma, Molecular-Sieving Energy-Efficient Gas Separation Membranes Enabled by multi-covalent-crosslinking of Microporous Polymer Blends, 2021.
[63] W. Ji, K. Li, W. Shi, L. Bai, J. Li, X. Ma, The effect of chain rigidity and microporosity on the sub-ambient temperature gas separation properties of intrinsic microporous polyimides, J. Membr. Sci. 635 (2021) 119439.
[64] X. Chen, Z. Zhang, L. Wu, X. Liu, S. Xu, J.E. Efome, X. Zhang, N. Li, Polymers of intrinsic microporosity having bulky substitutes and cross-linking for gas separation membranes, ACS Appl. Polym. Mater. 2 (2020) 987–995.
[65] I. Rose, M. Carta, R. Malpass-Evans, M.-C. Ferrari, P. Bernardo, G. Clarizia, J. C. Jansen, N.B. McKeown, Highly permeable benzotriptycene-based polymer of intrinsic microporosity, ACS Macro Lett. 4 (2015) 912–915.
[66] S.A. Felemban, C.G. Bezzu, B. Comesaña-Gándara, J.C. Jansen, A. Fuoco, E. Esposito, M. Carta, N.B. McKeown, Synthesis and gas permeation properties of tetraoxidethianthrene-based polymers of intrinsic microporosity, J. Mater. Chem. A 9 (2021) 2840–2849.
[67] M. Longo, B. Comesaña-Gándara, M. Monteleone, E. Esposito, A. Fuoco, L. Giorno, N.B. McKeown, J.C. Jansen, Matrimid® 5218/AO-PIM-1 blend membranes for gas separation, J. Membrane Sci. Res. 8 (2022).
[68] R. Swaidan, B.S. Ghanem, E. Litwiller, I. Pinnau, Pure-and mixed-gas CO2/CH4 separation properties of PIM-1 and an amidoxime-functionalized PIM-1, J. Membr. Sci. 457 (2014) 95–102.
[69] R. Swaidan, B. Ghanem, E. Litwiller, I. Pinnau, Physical aging, plasticization and their effects on gas permeation in "rigid" polymers of intrinsic microporosity, Macromolecules 48 (2015) 6553–6561.
[70] R. Swaidan, B. Ghanem, I. Pinnau, ACS Publications, 2015.
[71] Q. Li, Z. Zhu, Y. Wang, H. Wang, J. Li, X. Ma, Unprecedented gas separation performance of ITTB/CNT nanocomposite membranes at low temperature by strong interfacial interaction enhanced rigidity, J. Membr. Sci. 636 (2021) 119590.
[72] C.G. Bezzu, M. Carta, M.-C. Ferrari, J.C. Jansen, M. Monteleone, E. Esposito, A. Fuoco, K. Hart, T. Liyana-Arachchi, C.M. Colina, The synthesis, chain-packing simulation and long-term gas permeability of highly selective spirobifluorene-based polymers of intrinsic microporosity, J. Mater. Chem. A 6 (2018) 10507–10514.
[73] R.R. Tiwari, J. Jin, B. Freeman, D. Paul, Physical aging, CO2 sorption and plasticization in thin films of polymer with intrinsic microporosity (PIM-1), J. Membr. Sci. 537 (2017) 362–371.
[74] Ş.B. Tantekin-Ersolmaz, Ç. Atalay-Oral, M. Tatlıer, A. Erdem-Şenatalar, B. Schoeman, J. Sterte, Effect of zeolite particle size on the performance of polymer–zeolite mixed matrix membranes, J. Membr. Sci. 175 (2000) 285–288.
[75] G. Clarizia, C. Algieri, E. Drioli, Filler-polymer combination: a route to modify gas transport properties of a polymeric membrane, Polymer 45 (2004) 5671–5681.
[76] J.-M. Duval, B. Folkers, M. Mulder, G. Desgrandchamps, C. Smolders, Adsorbent filled membranes for gas separation. Part 1. Improvement of the gas separation properties of polymeric membranes by incorporation of microporous adsorbents, J. Membr. Sci. 80 (1993) 189–198.
[77] M. Jia, K.-V. Peinemann, R.-D. Behling, Molecular sieving effect of the zeolite-filled silicone rubber membranes in gas permeation, J. Membr. Sci. 57 (1991) 289–292.
[78] S. Stern, V. Shah, B. Hardy, Structure-permeability relationships in silicone polymers, J. Polym. Sci. B Polym. Phys. 25 (1987) 1263–1298.
[79] L. Xiang, D. Liu, H. Jin, L.-W. Xu, C. Wang, S. Xu, Y. Pan, Y. Li, Locking of phase transition in MOF ZIF-7: improved selectivity in mixed-matrix membranes for O 2/N 2 separation, Mater. Horiz. 7 (2020) 223–228.
[80] Y. Mansourpanah, F. Bagri, Improvement of the performance of PDMS top layer of mixed matrix membrane incorporated with treated ZIF-8 for gas separation, J. Membrane Sci. Res. 7 (2021) 111–117.
[81] M.A. Semsarzadeh, M. Ghahramani, Synthesis and morphology of polyacrylate-poly (dimethyl siloxane) block copolymers for membrane application, Macromol. Res. 23 (2015) 898–908.
[82] H.B. Park, J.K. Kim, S.Y. Nam, Y.M. Lee, Imide-siloxane block copolymer/silica hybrid membranes: preparation, characterization and gas separation properties, J. Membr. Sci. 220 (2003) 59–73.
[83] Y. Bum, L. Ho, B. Park, J. Kie, S. Young, M. Lee, Synthesis and characterization of polyamideimide-branched siloxane and its gas-separation, J. Appl. Polym. Sci. 74 (1999) 965–973.
[84] S.Y. Ha, H.B. Park, Y.M. Lee, Percolational effect of siloxane content in poly (amideimide siloxane) on the gas permeation behavior, Macromolecules 32 (1999) 2394–2396.
[85] H.B. Park, S.Y. Ha, Y.M. Lee, Percolation behavior of gas permeability in rigid-flexible block copolymer membranes, J. Membr. Sci. 177 (2000) 143–152.
[86] Y. Nagase, T. Ando, C.M. Yun, Syntheses of siloxane-grafted aromatic polymers and the application to pervaporation membrane, Reactive Funct. Polym. 67 (2007) 1252–1263.
[87] C. Joly, M. Smaihi, L. Porcar, R. Noble, Polyimide– silica composite materials: how does silica influence their microstructure and gas permeation properties? Chem. Mater. 11 (1999) 2331–2338.
[88] H.B. Park, C.K. Kim, Y.M. Lee, Gas separation properties of polysiloxane/polyether mixed soft segment urethane urea membranes, J. Membr. Sci. 204 (2002) 257–269.
[89] Y. Nagase, A. Naruse, K. Matsui, Chemical modification of polysulphone: 2. Gas and liquid permeability of polysulphone/polydimethylsiloxane graft copolymer membranes, Polymer 31 (1990) 121–125.
[90] S. Kim, T.W. Pechar, E. Marand, Poly (imide siloxane) and carbon nanotube mixed matrix membranes for gas separation, Desalination 192 (2006) 330–339.
[91] E. Roh, I. Subiyanto, W. Choi, Y.C. Park, C.H. Cho, H. Kim, CO2/N2 and O2/N2 separation using mixed-matrix membranes with MOF-74 nanocrystals synthesized via microwave reactions, Bull. Kor. Chem. Soc. 42 (2021) 459–462.
[92] S. Xu, W. Ma, H. Zhou, Y. Zhang, H. Jia, J. Xu, P. Jiang, X. Wang, W. Zhao, A novel imide-bridged polysiloxane membrane was prepared via one-pot hydrosilylation reaction for O2/N2 separation, ACS Omega 6 (2021) 19553–19558.
[93] D.T. Clausi, S.A. McKelvey, W.J. Koros, Characterization of substructure resistance in asymmetric gas separation membranes, J. Membr. Sci. 160 (1999) 51–64.
[94] S. Kim, L. Chen, J.K. Johnson, E. Marand, Polysulfone and functionalized carbon nanotube mixed matrix membranes for gas separation: theory and experiment, J. Membr. Sci. 294 (2007) 147–158.
[95] S.S. Swain, L. Unnikrishnan, S. Mohanty, S.K. Nayak, Hybridization of MWCNTs and reduced graphene oxide on random and electrically aligned nanocomposite membrane for selective separation of O2/N2 gas pair, J. Mater. Sci. 53 (2018) 15442–15464.
[96] J. Ahn, W.-J. Chung, I. Pinnau, M.D. Guiver, Polysulfone/Silica nanoparticle mixed-matrix membranes for gas separation, J. Membr. Sci. 314 (2008) 123–133.
[97] S. Shafiq, B.A. Al-Maythalony, M. Usman, M.S. Ba-Shammakh, A.A. Al-Shammari, ZIF-95 as a filler for enhanced gas separation performance of polysulfone membrane, RSC Adv. 11 (2021) 34319–34328.
[98] A. Ismail, W. Rahman, F. Aziz, AIP Conference Proceedings, American Institute of Physics, 2009, pp. 201–206.
[99] Y. Dai, M.D. Guiver, G.P. Robertson, Y.S. Kang, K.J. Lee, J.Y. Jho, Preparation and characterization of polysulfones containing both hexafluoroisopropylidene and trimethylsilyl groups as gas separation membrane materials, Macromolecules 37 (2004) 1403–1410.
[100] A. Lewisky, H. Ibrahimov,Gas separation using polysulfone membranes optimized with nanoparticles, methods (cryogenic distillation, amine-based absorption and, Press. swing Adsorpt., 1 5.
[101] H. Wang, B.A. Holmberg, Y. Yan, Homogeneous polymer–zeolite nanocomposite membranes by incorporating dispersible template-removed zeolite nanocrystals, J. Mater. Chem. 12 (2002) 3640–3643.
[102] A. Zulhairun, A. Ismail, The role of layered silicate loadings and their dispersion states on the gas separation performance of mixed matrix membrane, J. Membr. Sci. 468 (2014) 20–30.
[103] B.D. Reid, F.A. Ruiz-Trevino, I.H. Musselman, K.J. Balkus, J.P. Ferraris, Gas permeability properties of polysulfone membranes containing the mesoporous molecular sieve MCM-41, Chem. Mater. 13 (2001) 2366–2373.
[104] G. Kapantaidakis, S. Kaldis, X. Dabou, G. Sakellaropoulos, Gas permeation through PSF-PI miscible blend membranes, J. Membr. Sci. 110 (1996) 239–247.
[105] P.P. Patil, B. Sreekant, S. Gurlhosur, A Study Effect of Perambilty and Selectivity on Mixed Matrix Membranes Made with Zeolite 4A in Polyethersulfone (PES)/polysulfone (PSF) for Gas Separation, 2022.
[106] H. Savoji, D. Rana, T. Matsuura, M. Soltanieh, S. Tabe, Novel surface modifying macromolecules (SMMs) blended polysulfone gas separation membranes by phase inversion technique, J. Appl. Polym. Sci. 124 (2012) 2287–2299.
[107] J. McHattie, W.J. Koros, D.R. Paul, Gas transport properties of polysulphones: 1. Role of symmetry of methyl group placement on bisphenol rings, Polymer 32 (1991) 840–850.
[108] C. Camacho-Zuñiga, F. Ruiz-Treviño, S. Hernández-López, M. Zolotukhin, F. Maurer, A. González-Montiel, Aromatic polysulfone copolymers for gas separation membrane applications, J. Membr. Sci. 340 (2009) 221–226.
[109] C. Aitken, W.J. Koros, D.R. Paul, Gas transport properties of biphenol polysulfones, Macromolecules 25 (1992) 3651–3658.
[110] M.G. Süer, N. Baç, L. Yilmaz, Gas permeation characteristics of polymer-zeolite mixed matrix membranes, J. Membr. Sci. 91 (1994) 77–86.
[111] Y. Li, T.-S. Chung, C. Cao, S. Kulprathipanja, The effects of polymer chain rigidification, zeolite pore size and pore blockage on polyethersulfone (PES)-Zeolite A mixed matrix membranes, J. Membr. Sci. 260 (2005) 45–55.
[112] Y. Li, H.-M. Guan, T.-S. Chung, S. Kulprathipanja, Effects of novel silane modification of zeolite surface on polymer chain rigidification and partial pore

blockage in polyethersulfone (PES)–Zeolite A mixed matrix membranes, J. Membr. Sci. 275 (2006) 17–28.
[113] W.W. Lestari, R. Al Adawiyah, M.A. Khafidhin, R. Wijiyanti, N. Widiastuti, D. S. Handayani, CO2 gas separation using mixed matrix membranes based on polyethersulfone/MIL-100 (al), Open Chem. 19 (2021) 307–321.
[114] N.B. Ridzuan, M.H. Musa, Comparison between treated and untreated zeolite towards the performance of polyethersulfone mixed matrix membranes (MMMs) for O2/N2 gas separation, Adv. Mater. Res. 550 (2012) 728–735.
[115] T.D. Kusworo, A.F. Ismail, A. Mustafa, Hybrid membrane using polyethersulfone-modification of multiwalled carbon nanotubes with silane agent to enhance high performance oxygen separation, Int. J. Sci. Eng. 6 (2014) 163–168.
[116] S. Zeinali, M. Aryaeinezhad, Improving O2/N2 selective filtration using carbon nanotube-modified mixed-matrix membranes, Chem. Eng. Technol. 38 (2015) 2079–2086.
[117] A. Ismail, R. Rahim, W. Rahman, Characterization of polyethersulfone/ Matrimid® 5218 miscible blend mixed matrix membranes for O2/N2 gas separation, Separ. Purif. Technol. 63 (2008) 200–206.
[118] S. Madaeni, M. Esmaeili, S. Attar Nosrati, J. Barzin, Preparation and characterization of PES and PA composite membranes for air separation at low pressures, Int. Polym. Process. 28 (2013) 281–290.
[119] S. Madaeni, M. Esmaeili, J. Barzin, Preparation and optimisation of polyethersulfone-based composite membranes for air separation at low pressures, Polym. Polym. Compos. 15 (2007) 579–589.
[120] Z. Liu, B. Liu, L. Li, Y. Zhang, Z. Jiang, Synthesis of novel poly (Aryl ether sulfone) s bearing bulky pendants for gas separation membranes, Macromol. Res. 21 (2013) 608–613.
[121] K. Zarshenas, A. Raisi, A. Aroujalian,Surface Modification of Dual-Layer Polyamide6/Polyethersulfone Membrane by Corona Air Plasma for Gas Separation.
[122] R.S. Murali, T. Sankarshana, S. Sridhar, A. Kharitonov, Fluorinated polymer membranes for separation of industrial gas mixtures, J. Polym. Mater. 29 (2012) 317–330.
[123] M. Zarabadipoor, M. Shahrooz, N. Nasiri, M. Talebali, A. Mehrabani, S. Maghami, M. Sadeghi,Highly selective polyethersulfone/graphitic carbon nitride mixed matrix membranes for gas separation: the role of solvent-induced crystallization, Graphitic Carbon Nitride Mixed Matrix Membranes for Gas Separation: the Role of Solvent-Induced Crystallization.
[124] Z. Cheng, P. Wang, Y. Sun, Z. Wang, G. Zhou, Solvent-induced microphase separation membranes of block poly (Aryl ether sulfone) copolymer with high selectivity of O2/N2 separation, Polymer 297 (2024) 126867.
[125] R.S. Murali, S. Sridhar, T. Sankarshana, Y. Ravikumar, Gas permeation behavior of Pebax-1657 nanocomposite membrane incorporated with multiwalled carbon nanotubes, Ind. Eng. Chem. Res. 49 (2010) 6530–6538.
[126] J.H. Kim, Y.M. Lee, Gas permeation properties of poly (amide-6-b-ethylene oxide)–silica hybrid membranes, J. Membr. Sci. 193 (2001) 209–225.
[127] E. Esposito, R. Bruno, M. Monteleone, A. Fuoco, J. Ferrando Soria, E. Pardo, D. Armentano, J.C. Jansen, Glassy PEEK-WC vs. rubbery pebax® 1657 polymers: effect on the gas transport in CuNi-MOF based mixed matrix membranes, Appl. Sci. 10 (2020) 1310.
[128] M.S. Maleh, A. Raisi, Superior performance of surface-treated NaX@ Pebax-1657 membranes for O 2/N 2 separation, RSC Adv. 10 (2020) 17061–17069.
[129] M.S. Maleh, A. Raisi, Comparison of porous and nonporous filler effect on performance of poly (ether-block-amide) mixed matrix membranes for gas separation applications, Chem. Eng. Res. Des. 147 (2019) 545–560.
[130] K. Zarshenas, A. Raisi, A. Aroujalian, Mixed matrix membrane of nano-zeolite NaX/poly (ether-block-amide) for gas separation applications, J. Membr. Sci. 510 (2016) 270–283.
[131] R.S. Murali, A. Ismail, M. Rahman, S. Sridhar, Mixed matrix membranes of Pebax-1657 loaded with 4A zeolite for gaseous separations, Separ. Purif. Technol. 129 (2014) 1–8.
[132] P.D. Sutrisna, J. Hou, H. Li, Y. Zhang, V. Chen, Improved operational stability of Pebax-based gas separation membranes with ZIF-8: a comparative study of flat sheet and composite hollow fibre membranes, J. Membr. Sci. 524 (2017) 266–279.
[133] S. Habibiannejad, A. Aroujalian, A. Raisi, Pebax-1657 mixed matrix membrane containing surface modified multi-walled carbon nanotubes for gas separation, RSC Adv. 6 (2016) 79563–79577.
[134] L. Wang, P. Ji, Y. Li, M. Di, Q. Lv, S. Li, Design of poly (ether block amide)/ polyacrylonitrile composite membrane for carbon dioxide capture, Functional Mater. Lett. 8 (2015) 1550045.
[135] H. Nagar, P. Vadthya, N.S. Prasad, S. Sridhar, Air separation by facilitated transport of oxygen through a pebax membrane incorporated with a cobalt complex, RSC Adv. 5 (2015) 76190–76201.
[136] J. Lai, S. Wei, Preparation of vinylpyridine irradiation-grafted poly (4-methyl-pentene-1) membrane for oxygen enrichment, J. Appl. Polym. Sci. 32 (1986) 5763–5775.
[137] A. Alihosseini, A. Hedayati Moghaddam, Permeability and selectivity prediction of poly (4-methyl 1-pentane) membrane modified by nanoparticles in gas separation through artificial intelligent systems, Polyolefins J. 7 (2020) 91–98.
[138] A. Alihosseini, D. Zergani, A.H. Saeedi Dehaghani, Optimization of parameters affecting separation of gas mixture of O2, N2, CO2 and CH4 by PMP membrane modified with TiO2, ZnO and Al2O3 nanoparticles, Polyolefins J. 7 (2019) 13–24.
[139] S.Y. Markova, N. Smirnova, V. Teplyakov, Gas permeability through poly (4-methyl-1-pentene) at temperatures above and below the glass transition point, Petrol. Chem. 56 (2016) 948–955.
[140] F.-C. Lin, D.-M. Wang, J.-Y. Lai, Asymmetric TPX membranes with high gas flux, J. Membr. Sci. 110 (1996) 25–36.
[141] A. Tanioka, Separation of gases by polymer membranes, Int. J. Polym. Mater. 20 (1993) 261–264.
[142] J. Lai, J. Shieh, S. Shyu, MMA/TPX homograft membrane for oxygen enrichment, J. Appl. Polym. Sci. 37 (1989) 2907–2919.
[143] J.-M. Levaesalmi, T.J. McCarthy, Gas permeability of surface-selectively chlorinated poly (4-methyl-1-pentene), Macromolecules 28 (1995) 1733–1738.
[144] J. Lai, G. Wu, S. Shyu, TPX/Siloxane blend membrane for oxygen enrichment, J. Appl. Polym. Sci. 34 (1987) 559–569.
[145] J. Lai, C. Shih, F. Lin, Plasma deposition of vinyl monomers onto poly (4-methyl-1-pentene)/poly (Dimethyl siloxane) blend membrane for enrichment of oxygen from air, Polym. J. 26 (1994) 665–674.
[146] M.H. Nematollahi, S. Babaei, R. Abedini, CO 2 separation over light gases for nano-composite membrane comprising modified polyurethane with SiO 2 nanoparticles, Kor. J. Chem. Eng. 36 (2019) 763–779.
[147] Z.F. Wang, B. Wang, Y.R. Yang, C.P. Hu, Correlations between gas permeation and free-volume hole properties of polyurethane membranes, Eur. Polym. J. 39 (2003) 2345–2349.
[148] J. De Sales, P. Patrício, J. Machado, G. Silva, D. Windmöller, Systematic investigation of the effects of temperature and pressure on gas transport through polyurethane/poly (methylmethacrylate) phase-separated blends, J. Membr. Sci. 310 (2008) 129–140.
[149] M.A. Semsarzadeh, B. Ghalei, Characterization and gas permeability of polyurethane and polyvinyl acetate blend membranes with polyethylene oxide–polypropylene oxide block copolymer, J. Membr. Sci. 401 (2012) 97–108.
[150] P. Patricio, J. De Sales, G. Silva, D. Windmöller, J. Machado, Effect of blend composition on microstructure, morphology, and gas permeability in PU/PMMA blends, J. Membr. Sci. 271 (2006) 177–185.
[151] D. Gomes, K.-V. Peinemann, S. Nunes, W. Kujawski, J. Kozakiewicz, Gas transport properties of segmented poly (ether siloxane urethane urea) membranes, J. Membr. Sci. 281 (2006) 747–753.
[152] S.-H. Chen, K.-C. Yu, S.-L. Houng, J.-Y. Lai, Gas transport properties of HTPB based polyurethane/cosalen membrane, J. Membr. Sci. 173 (2000) 99–106.
[153] P. Knight, D. Lyman, Gas permeability of various block Copolyether—Urethanes, J. Membr. Sci. 17 (1984) 245–254.
[154] M. Pegoraro, L. Zanderighi, A. Penati, F. Severini, F. Bianchi, N. Cao, R. Sisto, C. Valentini, Polyurethane membranes from polyether and polyester diols for gas fractionation, J. Appl. Polym. Sci. 43 (1991) 687–697.
[155] K. Madhavan, D. Gnanasekaran, B.S. Reddy, Poly (dimethylsiloxane-urethane) membranes: effect of linear siloxane chain and caged silsesquioxane on gas transport properties, J. Polym. Res. 18 (2011) 1851–1861.
[156] L.-S. Teo, C.-Y. Chen, J.-F. Kuo, The gas transport properties of amine-containing polyurethane and poly (urethane-urea) membranes, J. Membr. Sci. 141 (1998) 91–99.
[157] K.-H. Hsieh, C. Tsai, D. Chang, Vapor and gas permeability of polyurethane membranes. Part II. Effect of functional group, J. Membr. Sci. 56 (1991) 279–287.
[158] S. Matavos-Aramyan, M.H. Jazebizadeh, S. Babaei, Investigating CO2, O2 and N2 permeation properties of two new types of nanocomposite membranes: polyurethane/silica and polyesterurethane/silica, Nano-Struct. Nano-Objects 21 (2020) 100414.
[159] S. Tourani, F. Akbarbandari, Investigation of the gas separation properties of polyurethane membranes in presence of boehmite nanoparticles, J. Inorg. Organomet. Polym. Mater. 33 (2023) 61–75.
[160] Y. Yu, B. Liu, Y. Wang, S. Liu, X. Li, Z. Liu, Z. Jiang, Preparation of polyphenylsulfone containing imidazole group for gas separation membrane material, High Perform. Polym. 26 (2014) 401–407.
[161] M. Monteleone, R. Mobili, C. Milanese, E. Esposito, A. Fuoco, S. La Cognata, V. Amendola, J.C. Jansen, Peek–wc-based mixed matrix membranes containing polyimine cages for gas separation, Molecules 26 (2021) 5557.
[162] S. Samarasinghe, C.Y. Chuah, W. Li, G. Sethunga, R. Wang, T.-H. Bae, Incorporation of CoIII acetylacetonate and SNW-1 nanoparticles to tailor O2/N2 separation performance of mixed-matrix membrane, Separ. Purif. Technol. 223 (2019) 133–141.
[163] R.-C. Ruaan, T.-H. Wu, S.-H. Chen, J.-Y. Lai, Oxygen/Nitrogen separation by polybutadiene/polycarbonate composite membranes modified by ethylenediamine plasma, J. Membr. Sci. 138 (1998) 213–220.
[164] J.S. Chiou, D.R. Paul, Gas permeation in a dry nafion membrane, Ind. Eng. Chem. Res. 27 (1988) 2161–2164.
[165] J.-M. Yang, C.P.C. Chian, K.-Y. Hsu, Oxygen permeation in SBS-g-DMAEMA copolymer membrane prepared by UV photografting without degassing, J. Membr. Sci. 153 (1999) 175–182.
[166] T. Nakagawa, Y. Fujiwara, N. Minoura, Diffusivity and permeability of poly (α-amino acid) membranes to gases, J. Membr. Sci. 18 (1984) 111–127.
[167] J. Chiou, D. Paul, Gas permeation in miscible homopolymer–copolymer blends. I. Poly (Methyl methacrylate) and styrene/acrylonitrile copolymers, J. Appl. Polym. Sci. 34 (1987) 1037–1056.
[168] K. Min, D. Paul, Effect of tacticity on permeation properties of poly (methyl methacrylate), J. Polym. Sci. B Polym. Phys. 26 (1988) 1021–1033.
[169] M.H. Kim, J.H. Kim, C.K. Kim, Y.S. Kang, H.C. Park, J.O. Won, Control of phase separation behavior of PC/PMMA blends and their application to the gas separation membranes, J. Polym. Sci. B Polym. Phys. 37 (1999) 2950–2959.
[170] Z. Gao, B. Zhang, C. Yang, Y. Wu, Fabrication of CeO2/carbon molecular sieving membranes for enhanced O2/N2 gas separation, Appl. Surf. Sci. 649 (2024) 159127.

[171] E.T. Tikue, S.K. Kang, M.H. Kim, W.C. Kwak, I. An, S. Yang, J.-H. Kim, P.S. Lee, Mixed matrix membrane based on DOCDA polyimide with twisted kink structure and zeolite 4A for energy-efficient oxygen purification, J. Ind. Eng. Chem. 130 (2024) 612–622.
[172] S. Lv, X. Liu, J. Li, C. Gong, L. Wan, F. Huang, A new poly (trialkylsilylethynylphenylacetylene) s membrane toward enhanced oxygen permeability, J. Polym. Sci. 62 (2024) 1831–1841.
[173] X. Liu, Y. Wang, S. Liu, J. Luo, X. Zong, S. Xue, Tuning the fraction free volume of hyperbranched 6FDA/TAPA polyimide membrane via DAM for enhanced gas separation performance, Polym. Adv. Technol. 35 (2024) e6236.
[174] B.D. Cullity, C.D. Graham, Introduction to Magnetic Materials, John Wiley & Sons, 2011.
[175] C. Kittel, Introduction to Solid State Physics, eighth ed., 2021.
[176] G.L. Hornyak, J.J. Moore, H.F. Tibbals, J. Dutta, Fundamentals of Nanotechnology, CRC press, 2018.
[177] A. Rybak, A. Rybak, W. Kaszuwara, S. Boncel, Poly (2, 6-dimethyl-1, 4-phenylene oxide) hybrid membranes filled with magnetically aligned iron-encapsulated carbon nanotubes (fe@ MWCNTs) for enhanced air separation, Diam. Relat. Mater. 83 (2018) 21–29.
[178] T.M. Batrudinov, Y.E. Nekhoroshkova, E.I. Paramonov, V.S. Zverev, E. A. Elfimova, A.O. Ivanov, P.J. Camp, Dynamic magnetic response of a ferrofluid in a static uniform magnetic field, Phys. Rev. 98 (2018) 052602.
[179] A. Strzelewicz, Z.J. Grzywna, Studies on the air membrane separation in the presence of a magnetic field, J. Membr. Sci. 294 (2007) 60–67.
[180] S. Raveshiyan, S.S. Hosseini, J. Karimi-Sabet, Intensification of O2/N2 separation by novel magnetically aligned carbonyl iron powders/polysulfone magnetic mixed matrix membranes, Chem. Eng. Process. Process Intensif. 150 (2020) 107866.
[181] P. Borys, K. Pawelek, Z.J. Grzywna, On the magnetic channels in polymer membranes, Phys. Chem. Chem. Phys. 13 (2011) 17122–17129.
[182] G. Dudek, R. Turczyn, A. Strzelewicz, A. Rybak, M. Krasowska, Z.J. Grzywna, Preparation and characterization of iron oxides–polymer composite membranes, Separ. Sci. Technol. 47 (2012) 1390–1394.
[183] A. Rybak, W. Kaszuwara, Magnetic properties of the magnetic hybrid membranes based on various polymer matrices and inorganic fillers, J. Alloys Compd. 648 (2015) 205–214.
[184] M. Krasowska, A. Rybak, G. Dudek, A. Strzelewicz, K. Pawełek, Z.J. Grzywna, Structure morphology problems in the air separation by polymer membranes with magnetic particles, J. Membr. Sci. 415 (2012) 864–870.
[185] A. Strzelewicz, M. Krasowska, G. Dudek, A. Rybak, R. Turczyn, M. Cieśla, Anomalous Diffusion on Fractal Structure of Magnetic Membranes, 2013.
[186] A. Rybak, A. Strzelewicz, M. Krasowska, G. Dudek, Z.J. Grzywna, Influence of various parameters on the air separation process by magnetic membranes, Separ. Sci. Technol. 47 (2012) 1395–1404.
[187] A. Rybak, Z.J. Grzywna, P. Sysel, Mixed matrix membranes composed of various polymer matrices and magnetic powder for air separation, Separ. Purif. Technol. 118 (2013) 424–431.
[188] A. Rybak, G. Dudek, M. Krasowska, A. Strzelewicz, Z.J. Grzywna, Magnetic mixed matrix membranes consisting of PPO matrix and magnetic filler in gas separation, Separ. Sci. Technol. 49 (2014) 1729–1735.
[189] A. Rybak, A. Rybak, W. Kaszuwara, S. Awietjan, P. Sysel, Z.J. Grzywna, The studies on novel magnetic polyimide inorganic-organic hybrid membranes for air separation, Mater. Lett. 208 (2017) 14–18.
[190] A. Rybak, A. Rybak, W. Kaszuwara, S. Awietjan, J. Jaroszewicz, The rheological and mechanical properties of magnetic hybrid membranes for gas mixtures separation, Mater. Lett. 183 (2016) 170–174.
[191] A. Rybak, A. Rybak, W. Kaszuwara, S. Awietjan, R. Molak, P. Sysel, Z.J. Grzywna, The magnetic inorganic-organic hybrid membranes based on polyimide matrices for gas separation, Compos. B Eng. 110 (2017) 161–170.
[192] A. Rybak, A. Rybak, W. Kaszuwara, Characterization of selected parameters of organic-inorganic hybrid membranes based on various polymers and Nd-Fe-B fillers, Arch. Metall. Mater. 61 (2016) 1825–1832.
[193] A. Rybak, A. Rybak, W. Kaszuwara, M. Nyc, M. Auguścik, Metal substituted sulfonated poly (2, 6-dimethyl-1, 4-phenylene oxide) hybrid membranes with magnetic fillers for gas separation, Separ. Purif. Technol. 210 (2019) 479–490.
[194] X. Cao, R. Song, L. Zhang, F. Cheng, Z. Wang, Structurally ordered core-shell MOFs in mixed matrix membrane as magnetic sieves for O2/N2 separation, J. Membr. Sci. 698 (2024) 122624.
[195] N. Nady, N. Salem, S.H. Kandil, Novel magnetic iron–nickel/poly (ethersulfone) mixed matrix membranes for oxygen separation potential without applying an external magnetic field, Sci. Rep. 12 (2022) 13675.
[196] S. Ashtiani, J. Azadmanjiri, N.V. Hong, J. Floreková, C. Regmi, Z. Sofer, M. Khoshnamvand, K. Friess, Advancing high-performance mixed matrix membrane via magnetically aligned polycrystalline Co0. 5Ni0. 5FeCrO4 magnetic spinel nanoparticles for effective H2/CO2 and O2/N2 gas separation, Adv. Mater. Interfac. 9 (2022) 2201351.
[197] N. Nady, N. Salem, M.R. Elmarghany, M.S. Salem, S.H. Kandil, Novel magnetic mixed cellulose acetate matrix membranes with oxygen-enrichment potential, Membranes 12 (2022) 1259.
[198] H. Liu, C. Wang, Y. Qin, Y. Huang, C. Xiao, Oriented structure design and evaluation of Fe3O4/o-MWCNTs/PVC composite membrane assisted by magnetic field, J. Taiwan Inst. Chem. Eng. 120 (2021) 278–290.
[199] N. Fadaly, F. Aziz, Preparation and characterization of mixed matrix membrane based on polysulfone (PSF) and lanthanum orthoferrite (LaFeO3) for gas separation, J. Appli. Membrane Sci. Technol. 24 (2020).
[200] S.B. Park, P.W. Heo, The enhancement of oxygen separation from the air and water using poly (vinylidene fluoride) membrane modified with superparamagnetic particles, J. Membr. Sci. 466 (2014) 274–280.
[201] S. Raveshiyan, J. Karimi-Sabet, S.S. Hosseini, Influence of particle size on the performance of polysulfone magnetic membranes for O2/N2 separation, Chem. Eng. Technol. 43 (2020) 2437–2446.
[202] H. Zhao, F. Guo, X. Ding, X. Tan, Y. Zhang, An orderly-arranged Attapulgite/PIM-1 mixed matrix membranes for gas separation, Int. J. Nanosci. Nanotechnol. 19 (2023) 295–306.
[203] M. Tagirov, R. Aminova, G. Frossati, V. Efimov, G. Mamin, V. Naletov, D. Tayurskii, A. Yudin, On the magnetism of liquid nitrogen–liquid oxygen mixture, Phys. B Condens. Matter 329 (2003) 433–434.
[204] A. Rybak, G. Dudek, M. Krasowska, A. Strzelewicz, Z.J. Grzywna, P. Sysel, Magnetic mixed matrix membranes in air separation, Chem. Pap. 68 (2014) 1332–1340.
[205] A. Rybak, Z.J. Grzywna, W. Kaszuwara, On the air enrichment by polymer magnetic membranes, J. Membr. Sci. 336 (2009) 79–85.
[206] A. Rybak, M. Krasowska, A. Strzelewicz, Z.J. Grzywna, Smoluchowski type" equations for modelling of air separation by membranes with various structure, Acta Phys. Pol. B 40 (2009).